

# Theoretical Surface Science and Catalysis—Calculations and Concepts

B. HAMMER

*Institute of Physics*

*Aalborg University*

*DK-9220 Aalborg, Denmark*

AND

J. K. NØRSKOV

*Center for Atomic-Scale Materials Physics*

*Department of Physics*

*Technical University of Denmark*

*DK-2800 Lyngby, Denmark*

The application of density functional theory to calculate adsorption properties, reaction pathways, and activation energies for surface chemical reactions is reviewed. Particular emphasis is placed on developing concepts that can be used to understand and predict variations in reactivity from one transition metal to the next or the effects of alloying, surface structure, and adsorbate–adsorbate interactions on the reactivity. Most examples discussed are concerned with the catalytic properties of transition metal surfaces, but it is shown that the calculational approach and the concepts developed to understand trends in reactivity for metals can also be used for sulfide and oxide catalysts. © 2000 Academic Press.

## I. Introduction

When a solid catalyst is used to speed up a chemical process, the overall reaction usually consists of a series of elementary steps. These include

**Abbreviations:** B3LYP, Becke's hybrid description of exchange-correlation effects; bcc, body centred cubic; DFT, density functional theory; DOS, density of (one-electron) states; fcc, face centred cubic; GGA, generalized gradient approximation; hcp, hexagonal close packed; LDA, local density approximation; LEED, low energy electron diffraction; LMTO, linearized muffin tin orbital; PBE, Perdew, Burke, Ernzerhof exchange-correlation; PW91, Perdew, Wang 91 version of exchange-correlation; RPBE, Hammer, Hansen, Norskov modified PBE exchange-correlation; TS, transition state;  $E_{\text{chem}}$ , chemisorption energy;  $W$ , band width;  $\epsilon_F$ , fermi energy;  $\epsilon_d$ , center of  $d$ -band;  $\epsilon_a$ , adsorbate energy level;  $V$ , coupling matrix element;  $V_{ad}$ , adsorbate–metal  $d$  coupling matrix element;  $V_{dd}$ , metal  $d$ –metal  $d$  coupling matrix element;  $r$ , chemical reaction rate;  $v$ , frequency factor;  $E_a$ , activation energy;  $k$ , Boltzmann's constant;  $\Delta E_{\text{es}}$ , electrostatic energy difference;  $\sum_i \epsilon_i$ , sum of one-electron energies;  $\Delta E_{\text{dip}}$ , dipole–dipole interaction energy;  $\mu$ , dipole moment;  $E$ , electric field strength;  $E_{\text{segr}}$ , segregation energy.

adsorption of the reactants on the surface of the solid, diffusion on the surface, breaking of some reactant bonds, and the creation of new ones to form the product molecules, which eventually desorb from the surface. The complexity of these processes and of the catalysts makes it a demanding task to establish a molecular-level understanding of heterogeneous catalysis. The approach taken in surface science has been to study elementary reactions on well-defined single-crystal surfaces in order to build an understanding of some of the basic processes involved in catalysis. Single-crystal surfaces are only crude models of the high-surface-area catalysts used industrially. Catalysts need to have a high surface area, and they often consist of mixtures of phases, some of which have the catalytically active surface, whereas others support the small particles of active phases or keep them from sintering. Recently, the methods of surface science have developed further and it has become possible to produce and study models of supported catalysts and to investigate them under realistic high-pressure and -temperature conditions (1–8). This rapidly closes the gap between the surface science studies and studies of real catalysts. Simultaneously, the methods used to characterize high-surface-area catalysts have been refined considerably, and it has become possible to characterize the structure and other properties of the working catalysts *in situ* (9–12). Together, these different types of experiments have provided us with a wealth of detailed information about surface structures, adsorption geometries, bond strengths, and elementary reaction steps.

The rapidly increasing amount of data emphasizes the need for a conceptual framework for understanding or rationalizing the results. It would be extremely helpful to have an understanding of the most important factors determining the ability of a surface to bind or react with a particular molecule.

An important step toward a fundamental description of surface chemical processes has been taken recently with the development of quantum theoretical methods allowing us to calculate equilibrium structures, adsorption energies, reaction paths, and activation energies for simple processes on metal surfaces. The accuracy is still not sufficient to calculate rates of chemical reactions, but it is sufficient for a semiquantitative description of adsorption and reaction processes, and in particular for comparing different systems. The latter is particularly important if one wants theoretical input into a search for surfaces with a desired activity or selectivity for a given chemical reaction.

In this review, we discuss how the calculational methods in close conjunction with experiments can be used to develop some useful concepts to describe and understand adsorption and reactions on surfaces. We concentrate mainly on metal surfaces because this is the area in which both the experiments and the calculations are most advanced. Many of the concepts

developed for metal surfaces are more generally applicable also to semiconductors, oxides, and sulfides, and we illustrate this point at the end of this review. We show how we are beginning to understand which surface properties govern the variations in reactivity from one metal to the next and how adsorbate–adsorbate interactions, surface structure, strain, alloying, defects, and impurities may affect the reactivity.

The basis for our discussion of adsorbate–surface reactions is the density functional theory. We use density functional theory in accurate self-consistent calculations of adsorption properties and also as a basis for the development of models that discern the important physical quantities determining the reactivity of a given surface. We therefore start in Section II by giving a short description of the theoretical methods used and a discussion of their accuracy. We also discuss simple models of the electronic structure to be used in the following sections. In Section III, we discuss adsorption and surface reactions by treating in detail the simplest surface process, adsorption. We discuss in particular how the adsorption energy varies from one metal to the next. We also discuss the similar variation from one adsorbate to the next. We use the adsorption theory to introduce the parameters describing the surface which determine its ability to interact with an adsorbate. In Section IV we treat the more complex processes of molecules or atoms reacting on the surface. We focus in particular on trends in activation energies from one system to the next and show that the reactivity measures developed for simple atomic adsorption also work here. We use this as a starting point for a discussion in Section V of ways to change the reactivity of a given metal by changing the structure, by alloying, or by poisoning or promoting the surface by coadsorbed atoms and molecules. In Section VI, we summarize our results for metallic surfaces and establish a connection to the field of nonmetal catalysis.

## II. Theory of Adsorbate–Surface Interactions

The theoretical description of adsorbate–surface interactions is divided into two levels: (i) the accurate, but computationally demanding, calculation of adsorption properties, and (ii) the model description which is approximate but computationally simple. The large-scale calculations can be viewed as computer experiments. They complement real experiments in several ways. Often, it is a good check of an experiment or an interpretation of an experiment to have a calculation for comparison. There are also cases for which the calculation is simpler than the experiment. For example, consider an important fundamental property of a surface such as the surface energy. It is very difficult to measure, and currently the best source of

surface energies is calculations, which have been performed for all the metals in the periodic table (13). Finally, the calculation can sometimes be performed for situations that are not realizable experimentally. For instance, it is very simple to change the lattice constant of a metal in a calculation and bring out the effect of strain on the reactivity without concern about the problems associated with straining a crystal in real life (14). The ability to use the computer experiments to test models and theories of catalysis has recently breathed new life into the development of models and understanding of catalysis. The models are needed to bring out the concepts around which our description and understanding of catalysis revolves. What are the parameters of a surface determining its ability to adsorb a molecule or let one molecule react with another? Why are some adsorbates more reactive than others on a given surface? It is not possible, or even desirable, to have to perform a complete calculation or an experiment for each new system considered. We would like to be able to understand directly how a change in the catalyst composition or structure should change its reactivity. The models are essential in bringing out this understanding.

In the following sections, we first discuss briefly the calculational strategies and the strengths and limitations of the calculations. We then introduce some simple models and concepts to be used in the rest of the review to discuss and understand and the results of the calculations.

#### A. DENSITY FUNCTIONAL THEORY CALCULATIONS

There are two basically different approaches to the calculation of the electronic structure and total energies of molecules and solids: the wave function-based methods (15) and the density functional theory (DFT) methods (16–18). The former, which can be very accurate if a high level of configuration interactions is included, is currently limited to 10–100 electrons. If we consider transition metal surfaces, this limits the number of atoms that can be treated to about 10 since each transition metal has on the order of 10 valence electrons. This generally makes these methods unattractive for routine treatments of the complex systems needed to model catalysts. There are elegant ways of embedding a very accurately described region into a less accurately described surrounding region, which can increase the system sizes and make wave function-based methods very useful (19). The computational cost of such calculations and the limited size of systems that can be treated mean that, in a surface science and catalysis context, they are primarily useful as benchmarks, which can be used to gauge the accuracy of the less computationally demanding DFT methods. In the following, we therefore concentrate on the DFT methods.

Density functional theory describes how the ground state electron density and total energy can be obtained by solving a set of one-electron Schrödinger equations (the Kohn–Sham equations) instead of the complicated many-electron Schrödinger equation. This results in an enormous computational simplification, and systems with more than 1000 electrons can be treated.

There are several different methods used to solve the Kohn–Sham equations. In short, they can be characterized by the model used to describe the surface, by the kind of basis set used, and by the approximation used in the treatment of exchange-correlation effects:

### 1. *The Model Used to Describe the Surface*

The calculations cannot describe all the atoms in a solid or a catalyst particle, and a strategy must be chosen to limit the number of atoms treated explicitly. Two basic types of methods exist:

- *Cluster methods*, which describe only a limited cluster of the surface atoms in the hope that the surface atoms farther away from the adsorbates of interest are not important.
- *Slab methods*, whereby the surface is described as a slab with a periodic structure along the surface. The size of the surface unit cell determines the computational effort, and in principle the unit cell should be chosen to be large enough so that the adsorbates in neighboring unit cells do not interact.

The two types of models are illustrated in Fig. 1. The slab method can be viewed as a particular choice for the boundary conditions in the cluster approach, which, however, is generally found to describe the surface properties better than the cluster approach for a given number of atoms in the super cell or the cluster, respectively. In both methods, only a finite number of atomic layers can be included, and this will always represent an approximation. In addition, there are Greens function-based methods which can, in principle, treat a single adsorbate on a semi-infinite substrate (20–22), but they are not widely used.

### 2. *The Basis Set*

Two basic types of basis sets are most widely used:

- *Localized functions* [gaussians, atomic orbitals, linearized muffin tin orbitals (LMTOs), etc.]
- *Plane waves* [including augmented plane waves (LAPWs), etc.]

The choice depends on preference and the kind of problem studied. Localized functions are thus the usual choice in cluster-type models,

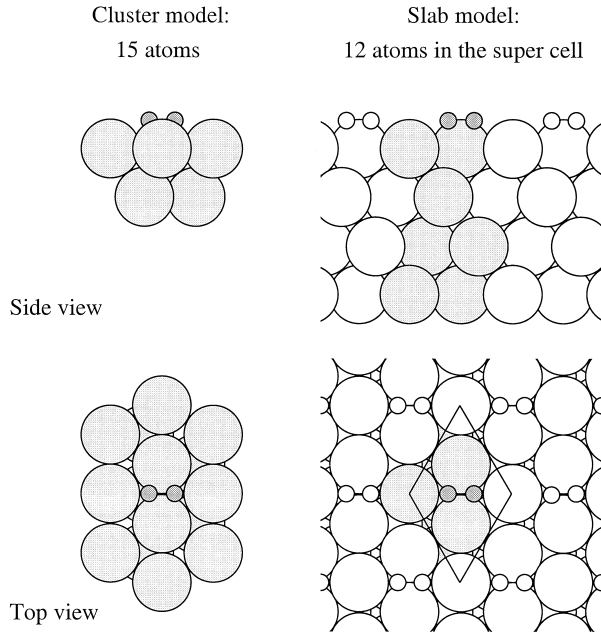


FIG. 1. Illustration of cluster and slab representations of an H<sub>2</sub> molecule (small circles) interacting with a semi-infinite surface. Replicas of the super cell atoms are shown with open circles.

whereas both localized (LMTOs) and plane waves are used in slab-type calculations. Usually, the core electrons are not treated explicitly, but instead are included as “frozen” or through a pseudopotential description of the ionic core (23). There are also elegant methods whereby the localized states are projected out and treated differently from the valence electrons (24).

### 3. The Description of Exchange Correlation

The error made by the choice of model used to describe the surface or the basis set can be controlled by increasing the size up to the point of convergence. This leaves the choice of exchange correlation functional as the main approximation in the DFT calculations. The most accurate method for treating exchange and correlation is probably Becke’s hybrid description of exchange-correlation effects (B3LYP) (25). In this method, a Hartree–Fock calculation is performed to derive the exact exchange energy, which is mixed with the DFT-based exchange energy. This hybrid method is therefore computationally very demanding. Less computationally

demanding are calculations which make use of one form or another of the generalized gradient approximation (GGA) (26–28). As illustrated in Table I, different GGA flavors can give quite different adsorption energies—they all, however, represent a great improvement over the local density approximation (LDA) description of the adsorption bond (29–33). The variations between different GGAs may be viewed as the intrinsic uncertainty of these methods. Adsorption energies or energy barriers are therefore not

TABLE I  
*Calculated Chemisorption Energies as a Function of the Exchange-Correlation Energy Functional, Compared with Measured Chemisorption Energies<sup>a</sup>*

	$E_{\text{chem}}$				
	LDA	PW91	PBE	RPBE	$E_{\text{chem}}^{\text{exp}}$
O(fcc)/Ni(111)	-6.68	-5.38	-5.27	-4.77	-4.84
O(hol)/Ni(100)	-6.97	-5.66	-5.55	-5.03	-5.41
O(hol)/Rh(100)	-6.64	-5.34	-5.23	-4.71	-4.56
O(fcc)/Pd(111)	-5.34	-4.08	-3.98	-3.49	
O(hol)/Pd(100)	-5.39	-4.14	-4.04	-3.53	
$\sigma_O$	1.84	0.57	0.47	0.24	
CO(fcc)/Ni(111)	-2.85	-1.99	-1.88	-1.49	-1.35
CO(hol)/Ni(100)	-3.05	-2.11	-2.00	-1.58	-1.26
CO(brd)/Rh(100)	-3.02	-2.28	-2.16	-1.81	-1.19
CO(fcc)/Pd(111)	-2.95	-2.07	-1.96	-1.56	(-1.47)
CO(brd)/Pd(100)	-2.77	-1.98	-1.87	-1.50	-1.69
$\sigma_{\text{CO}}$	1.58	0.78	0.67	0.37	
	(1.49)	(0.64)	(0.54)	(0.23)	
NO(hol) <sup>b</sup> /Ni(100)	-6.31	-4.52	-4.41	-3.68	-3.99
NO(brd)/Rh(100)	-3.73	-2.76	-2.67	-2.28	
NO(fcc)/Pd(111)	-3.27	-2.20	-2.12	-1.67	(-1.86)
NO(hol)/Pd(100)	-3.19	-2.12	-2.04	-1.58	-1.61
$\sigma_{\text{NO}}$	1.98	0.52	0.43	0.22	
$\sigma_{\text{tot}}$	1.76	0.66	0.56	0.30	
	(1.76)	(0.58)	(0.48)	(0.23)	

<sup>a</sup> LDA is the local density approximation, and PW91 (Perdew, Wang 91 version of exchange correlation), PBE (Perdew, Burke, Ernzerhof exchange correlation), and RPBE (Hammer, Hansen, Nørshov modified PBE exchange correlation) are different GGAs. All values are in eV per adsorbate. The rms deviations for the calculated chemisorption energies for O, CO, and NO ( $\sigma_O$ ,  $\sigma_{\text{CO}}$ , and  $\sigma_{\text{NO}}$ , respectively) and for all three adsorbates ( $\sigma_{\text{tot}}$ ) have been compiled only against the highly accurate microcalorimetric experimental results from Brown *et al.* (34). Chemisorption energies derived from temperature-programmed desorption experiments are given in parentheses. The  $\sigma$  values in parentheses occur when the CO/Rh(100) data are neglected. The  $E_{\text{chem}}$  value is relative to atomic O in the gas phase. From Hammer *et al.* (28). <sup>b</sup> Dissociative adsorption.

determined with uncertainties less than about 0.25 eV or 25 kJ/mol. Fortunately, energy differences and variations among systems are usually more accurate than because the errors tend to cancel for like systems. This means that vibrational frequencies and structures are usually extremely good in any of the methods. It also means that trends are better, and this is what we mainly focus on.

### B. SIMPLE MODELS

We consider in this section the simplest one-electron description of the quantum mechanics of atoms and molecules interacting with a metal surface. The idea is not to give an accurate description (this was discussed previously) but instead to bring out the essential physics.

A one-electron state in an atom or molecule outside a metal surface will interact with all the valence states of the surface atoms. These states form a band or several bands of states. Figure 2 shows a typical density of states for a transition metal. The broad *s* band is half filled—all the transition metals have one *s* electron (in the metallic state)—and the *d* states are seen to form much narrower bands. The occupancy of the *d* bands varies along the transition metals as they shift through the Fermi level. The narrow *d* bands are a consequence of the small coupling matrix element  $V_{dd}$  between the localized *d* states; one of the important conclusions from tight binding theory is that the band width is proportional to  $V_{dd}$  (35).

Since *d* bands are narrow, the interaction of an adsorbate state with the *d* electrons of a surface often gives rise to bonding and antibonding states just as in a simple two-state problem. This is illustrated in Fig. 3, which also illustrates what happens in the case of interaction with a broad band such as the *s* band of a metal. The adsorbate state only broadens. The broad band limit with a single resonance is often called “weak chemisorp-

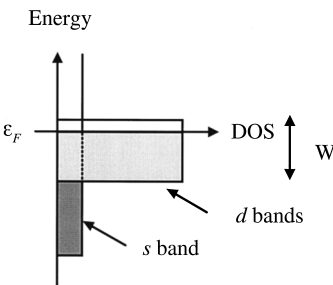


FIG. 2. Schematic illustration of the density of states of a transition metal, showing the broad *s* band and the narrow *d* bands (width  $W$ ) around the Fermi level,  $\varepsilon_F$ .

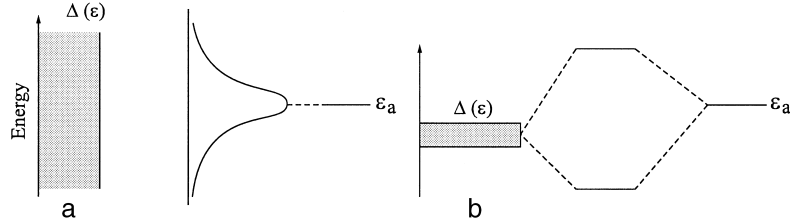


FIG. 3. The local density of states at an adsorbate in two limiting cases: (a) for a broad surface band; (b) for a narrow metal band. Case a corresponds to the interaction with a metal *s* band and case b is representative of the interaction with a transition metal *d* band.

tion,” whereas when there are split-off bonding and antibonding states we refer to “strong chemisorption” (36).

Figure 4 shows the result of a model calculation whereby a single adsorbate level is coupled by a matrix element  $V$  to a band of states. In the calculation,  $V$  is kept fixed as the band is shifted up in energy. The filling of the band is kept fixed so that as the center of the band  $\epsilon_d$  is shifted up toward the Fermi level, the band width  $W$  decreases. When the band is low and broad, only a single resonance can be seen at the bottom of the band, but as  $\epsilon_d$  shifts up a distinctive antibonding state appears above the band. Since these antibonding states are above the Fermi level, they are empty, and the bond becomes increasingly stronger as the number of empty antibonding states increases. The model calculation illustrates the transition between “weak” and “strong” chemisorption. The model calculation also illustrates a general principle about bonding at a surface: Strong bonding occurs if antibonding states are shifted up through the Fermi level (and become empty). The same is true if bonding states are shifted down through the Fermi level (and become filled). We use this general principle extensively in the following section.

### III. The Chemisorption Bond

In this section, we consider the bonding of an adsorbate to a surface. First, we discuss the simplest example of an atomic adsorbate and then increase the level of complexity by considering molecular adsorbates.

#### A. ATOMIC ADSORBATES

To illustrate the general quality of the DFT calculations for the calculation of chemisorption properties, consider as a first example oxygen adsorp-

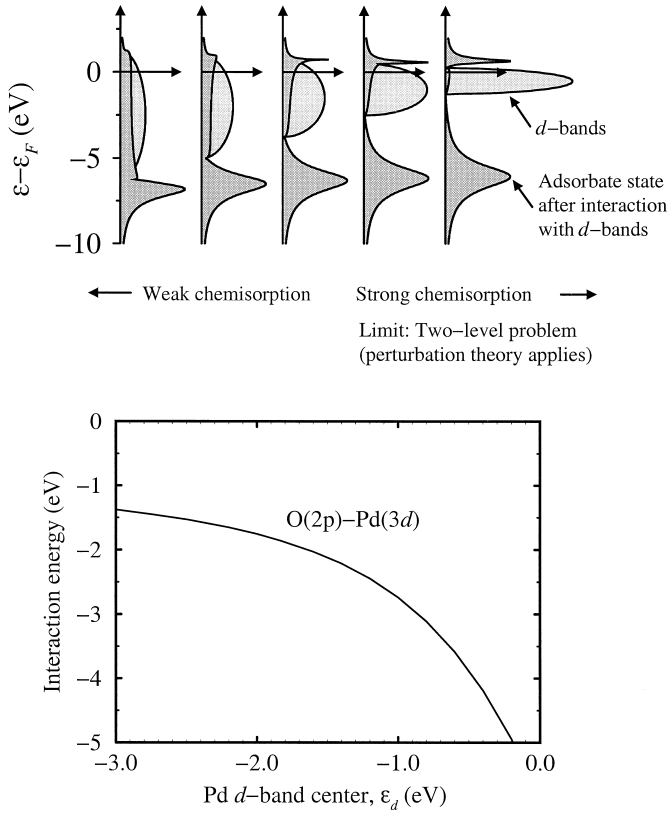
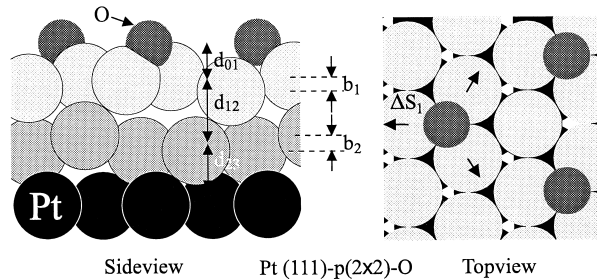


FIG. 4. The local density of states projected onto an adsorbate state interacting with the  $d$  bands at a surface. The strength of the adsorbate–surface coupling matrix element  $V$  is kept fixed as the center of the  $d$  bands  $\varepsilon_d$  is shifted up toward the Fermi energy ( $\varepsilon_F = 0$ ) and the width  $W$  of the  $d$  bands is decreased to keep the number of electrons in the bands constant. As  $\varepsilon_d$  shifts up, the antibonding states are emptied above  $\varepsilon_F$  and the bond becomes stronger (bottom). The calculation was done by using the Newns–Anderson model (37). Adapted from Hammer (38).

tion on the Pt(111) surface. This system has been studied in detail experimentally (39) and in several theoretical investigations (40, 41). We concentrate on the ordered  $p(2 \times 2)$  oxygen overlayer structure observed at a quarter of a monolayer of oxygen atoms. Figure 5 shows the geometry of this structure including relaxations of the platinum atoms at the surface and three layers down, as deduced from results of low-energy electron diffraction experiments. We also show the result of a DFT calculation (40). The equilibrium structure is determined by allowing all the coordinates of



	Experiment	Theory
$d_{01}$	1.18 Å	1.21 Å
$(d_{12} - d)/d$	1.3 %	0.6 %
$(d_{23} - d)/d$	0.0 %	-0.1 %
$b_1/d$	3.1 %	3.5 %
$b_2/d$	4.0 %	3.9 %
$\Delta S_1/S_1$	1.6 %	2.9 %

FIG. 5. The experimental and theoretical (PW91) equilibrium structure of the Pt(111)-p(2 × 2)-O system. From Hammer and Nørskov (40). The experimental results are from Starke *et al.* [39].

the atoms in the oxygen adlayer and in the two first layers to vary until the lowest-energy geometry is found. Clearly, all bond lengths and the relaxation pattern are reproduced by the calculation down to the 1% level.

The chemisorption potential energy, including relaxations of the platinum substrate, is calculated to be  $\Delta E_O = -4.29$  eV per oxygen atom relative to an atom in the gas phase [GGA and PW91 (Perdew, Wang 91 version of exchange correlation)]. The corresponding calculated bond energy per oxygen atom in  $O_2$  is 2.95 eV, so the heat of adsorption is -2.68 eV per molecule [the value found by using the RPBE (Hammer, Hansen, Nørskov modified PBE exchange correlation) functional would be 0.2–0.3 eV higher (28)]. This result is in reasonable agreement with results from microcalorimetry, which gives an integral heat of adsorption for a quarter of a monolayer of oxygen of about -2.4 eV/ $O_2$  (34).

We can also deduce the vibrational frequency for the oxygen vibration perpendicular to the surface. The experimental value is 58 meV (42), and the value calculated from the curvature of the total energy as a function of the height of the oxygen atoms above the surface is 59 meV.

To illustrate the variations in adsorption energies from one metal to the next, consider the adsorption of atomic oxygen on many transition metals

(Fig. 6). It is seen that copper, silver, and gold bind most weakly, and the unique nobleness of gold is clearly borne out. The O–Au surface bond is weaker than the O–O bond so that oxygen molecules will not readily dissociate on gold at all.

To understand the differences in chemisorption energy from one metal

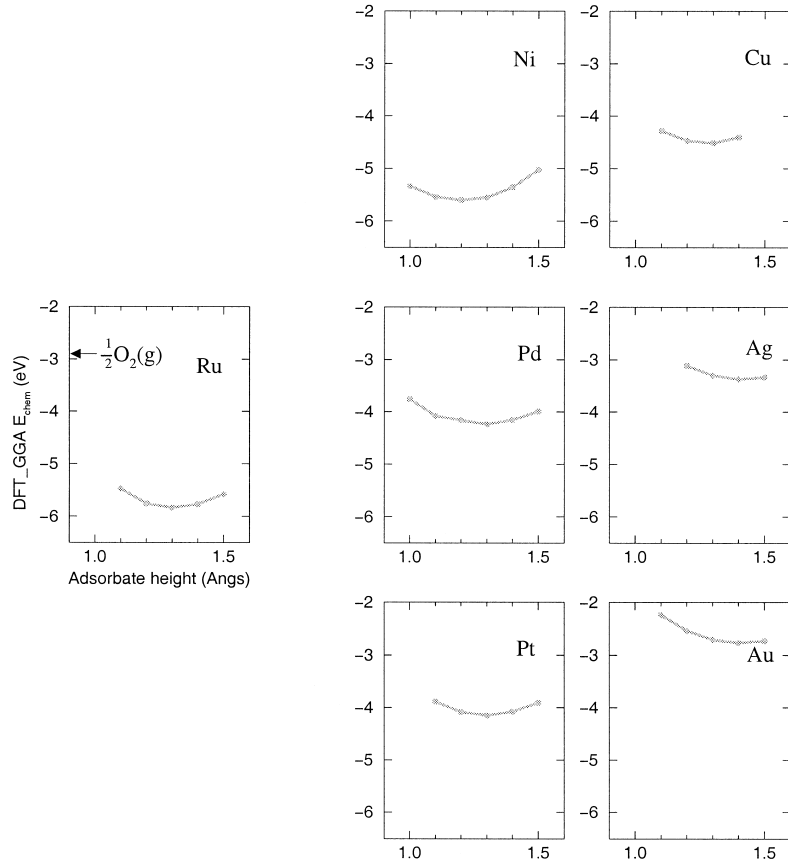


FIG. 6. Oxygen chemisorption at many close-packed late transition and noble metal surfaces {hexagonal close packed [hcp(0001)] for ruthenium, but face-centered cubic [fcc(111)] for the other metals}. A quarter monolayer of oxygen is adsorbed at the three-fold fcc site (the three-fold hcp for ruthenium) in a p (2 × 2) pattern. The adsorbate height is varied, and the metal ions are fixed at the truncated bulk positions. The chemisorption energy,  $E(O/\text{surface}) - E(O \text{ atom}) - E(\text{surface})$  is calculated by use of the PW91 functional. From Hammer and Nørskov (40).

to the next, consider in Fig. 7 the density of states projected onto one of the O  $2p$  states for oxygen chemisorbed on copper, silver, gold, nickel, palladium, platinum, and ruthenium. In each case, the density of states has a similar structure, and in Fig. 8 we show how one can think about the origin of the main peaks in the density of states. We imagine that the bond formation takes place in two steps (36, 40, 43). First, we let the adsorbate valence  $2p$  state that we consider interact with the metal  $s$  electrons. As discussed previously, this gives rise to a single resonance. All three oxygen  $2p$ -derived resonances are well below the Fermi level and hence completely

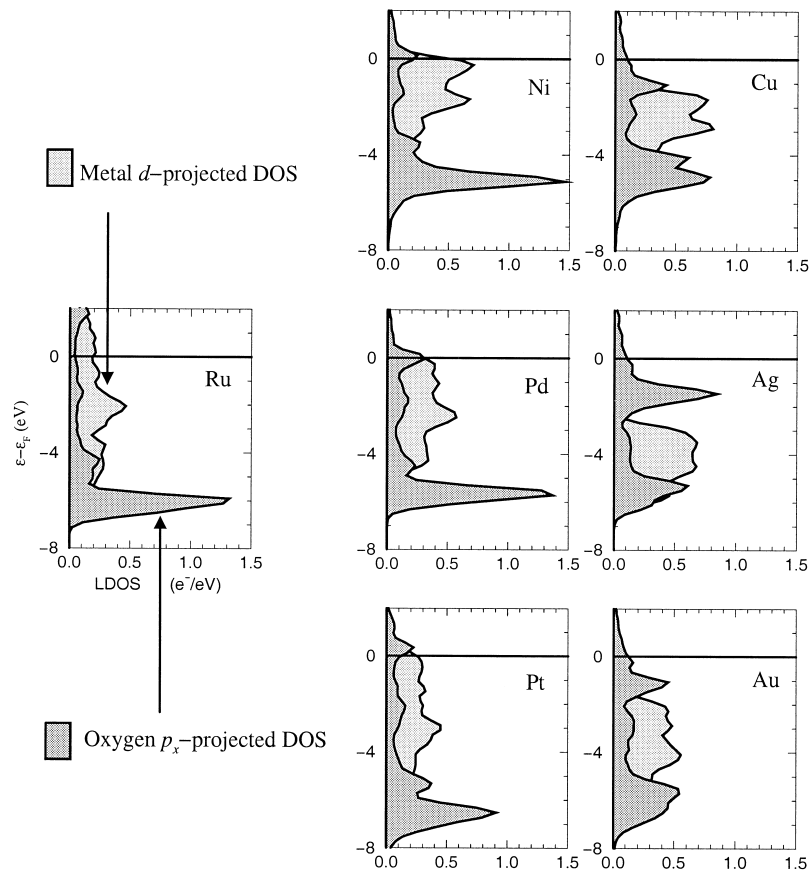


FIG. 7. Local density of states projected onto the oxygen  $2p_x$  state (dark-shaded area) for atomic oxygen 1.3 Å above close-packed surfaces of late transition metals (cf. Fig. 6). The light-shaded areas give the metal  $d$ -projected DOS for the respective metal surfaces before the oxygen chemisorption. From Hammer and Nørskov (40).

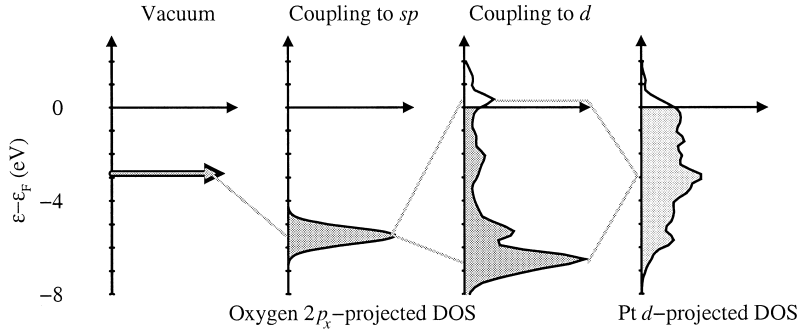


FIG. 8. Schematic illustration of the change in local electronic structure at an oxygen atom upon adsorption on simple and transition/noble metal surfaces. First, the sharp atomic states of the gas phase are broadened into resonances and shifted down due to the interaction with the metal *sp* states. Next, these renormalized states interact with the narrow *d* bands at the transition and noble metal surfaces, forming covalent bonding and antibonding states below and above the initial adsorbate and surface states. The coupling to the metal *d* electrons can roughly be viewed as a two-level coupling. The O/Pt(111) and Pt(111) DOS are from the self-consistent calculations in Fig. 7.

filled (one could say that the oxygen is in a  $2^-$  state). We then turn on the coupling to the *d* electrons. Since the *d* bands are narrow, this gives rise to strong interaction; that is, it gives rise to a splitting of the oxygen resonance into two: one state which is bonding with respect to the adsorbate and metal *d* states and another above the *d* bands which is antibonding.

The interpretation of the changes in electronic structure discussed previously has some immediate consequences for our understanding of the trends in the binding energies. We can also think of the binding energy as having two components—one from the coupling to the metal *s* states and one due to the extra coupling to the *d* states (36, 40, 43–45). Judging from the calculated densities of states in Fig. 7, we arrive at two conclusions: (i) The coupling to the *d* states is essentially a two-level problem giving rise to a bonding and an antibonding state, and (ii) the *d* bands can to a large extent be characterized by the band center,  $\varepsilon_d$ , only.

There are two general trends in Fig. 6 that must be explained. First in general, the farther to the left in the periodic table, the stronger the bond. Second, the farther down the periodic table, the weaker the interaction; the *5d* metals are more noble than the *4d* and *3d* metals.

To understand these two effects, we first note that since the contribution from the coupling to the metal *s* states is approximately the same for each of the metals considered, the main trends in the chemisorption energies should be given by the coupling to the *d* electrons (45).

The first effect is simple to understand in light of the previous discussion.

As we move to the left from copper, silver, or gold, the  $d$  bands move up in energy, and increasingly more antibonding adsorbate–metal  $d$  states become empty. This is clearly shown in Fig. 7. For copper, silver, and gold, the antibonding states are completely filled because the  $d$  bands are well below the Fermi level. As we move farther to the left in the  $3d$ ,  $4d$ , or  $5d$  series, the  $d$  bands shift up and the antibonding states become depopulated. The effect is illustrated more fully in Fig. 9, in which it is shown that the oxygen chemisorption energies become increasingly stronger as we move to the left in the  $4d$  transition metal series. Figure 9 includes experimental values, and the effect is evident in both the calculated and the measured values. In Fig. 9, it is also shown that the adsorption energy varies with the position of the  $d$  band center relative to the Fermi level, just as in the model calculation in Fig. 4, showing that the  $d$  band center is one possible measure of the reactivity of the transition metals. We note that the band

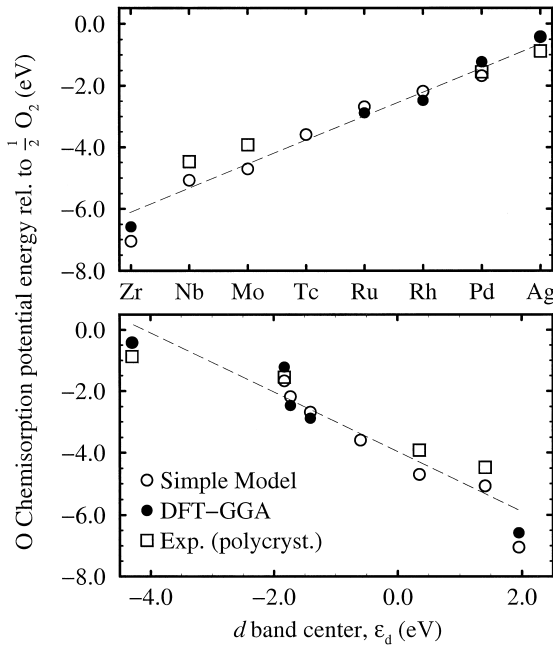


FIG. 9. Comparison of DFT-based oxygen chemisorption energies,  $E(O/\text{surface}) - \frac{1}{2}E(O_2) - E(\text{surface})$  (PW91), experimental values, and model estimates of the bond strengths for the various close-packed transition and noble metal surfaces. Data represented by open circles were determined by using the Newns–Anderson model. The experimental values are from Toyoshima and Somorjai (49). (Bottom) The calculated adsorption energies correlate well with the  $d$  band center  $\varepsilon_d$ .

center, the filling, and the width of the  $d$  bands vary through the  $4d$  series, i.e., the three quantities are strongly coupled. We choose to focus here on the band center, but we could also have chosen either of the other two parameters. It is shown below that this choice provides a very general picture. It is clear from the previous argument that the same trends should be expected of all simple atomic adsorbates with a filled valence level (after interaction with the metal  $s$  band), including hydrogen, carbon, nitrogen, fluorine, sulfur, and chlorine (40, 46–48).

To understand the second effect a slightly deeper analysis is required. We start by considering copper, silver, and gold, each of which has a filled  $d$  band and, according to Fig. 7, a negligible contribution to the bonding from the emptying of antibonding oxygen  $2p$ –metal  $d$  states. There is, however, still a contribution from the interaction between the metal  $d$  electrons and the oxygen  $2p$  states. The Pauli principle states that no two electrons can be in the same state, which means that the oxygen  $2p$  states have to become orthogonal to the metal  $d$  states when they come into contact (40, 46). This raises the kinetic energy by an amount that is approximately proportional to the square of the adsorbate–metal  $d$  coupling matrix element  $V_{ad}^2$ ; the stronger the overlap, the larger the repulsion.

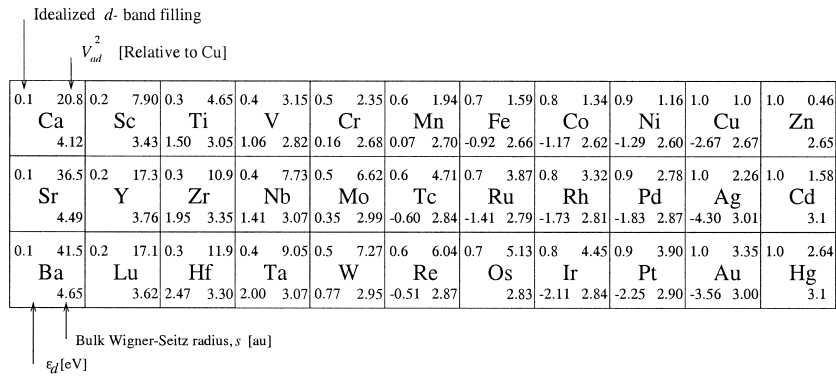


FIG. 10. Section of the periodic table with the  $3d$ ,  $4d$ , and  $5d$  transition metals. Shown in the lower right corner for each element is bulk Wigner–Seitz radius,  $s$ . In the lower left corner, the center of the  $d$  band is calculated for the most close-packed surface for each of the metals [(111) for fcc, (001) for hcp, and (110) for bcc]. In the upper right corner is shown the behavior of the adsorbate ( $s$  or  $p$ )–metal  $d$ -coupling matrix element squared,  $V_{ad}^2$ . The  $V_{ad}^2$ 's generally decrease for increasing nuclear charge within a row and increase down the groups. All the values, except for the properties of zinc, cadmium, and mercury were compiled from Andersen *et al.* (50). In the upper left corner, the idealized  $d$  band fillings are shown. These are similar to the actual, calculated bulk  $d$  band fillings considering the uncertainties in interpreting them (50).

The absolute magnitude of  $V_{ad}^2$  depends on the metal, the adsorbate, and the position of the adsorbate relative to the metal, but for a given adsorbate and a fixed adsorbate geometry the variations of the matrix element depend only on the extent of the metal  $d$  states. The variation in  $V_{ad}^2$  from one metal to the next for a fixed adsorbate and adsorbate geometry is therefore a property of the metal. For each element we know the *relative* strength of the coupling matrix element directly from tabulated values of the LMTO potential functions (40, 50). The values are shown in Fig. 10 for a large section of the periodic table.

Using the data in Fig. 10, we can test the hypothesis that the variation in adsorption strength from copper to gold is given mainly by the Pauli repulsion. In Fig. 11 we plot the calculated bond energies as a function of  $V_{ad}^2$ , and the proportionality is clearly seen. Gold has the most extended  $d$  states, the largest  $V_{ad}^2$ , and therefore the largest repulsion. This makes oxygen least stable on gold, and thus gold is the most noble metal (46). The same is true for hydrogen (46) and sulfur (40) and should, according to the model, hold for other electronegative adsorbates (such as the halogens) with deep-lying valence states after coupling with the metal  $sp$  states. For carbon and nitrogen, the picture is very similar, but here the adsorbate va-

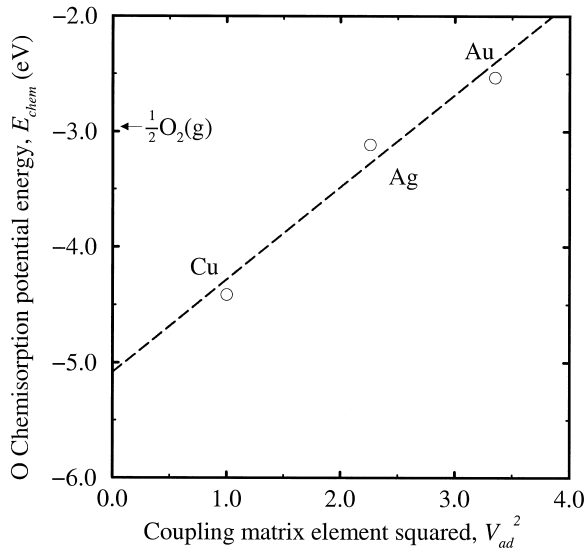


FIG. 11. The calculated chemisorption energy,  $E_{chem}$ , for  $\frac{1}{4}$  ML oxygen on Cu(111), Ag(111), and Au(111) (cf. Fig. 6) plotted versus the coupling matrix elements squared,  $V_{ad}^2$ , from Fig. 10. The proportionality confirms that the variations in bond strength are given by the strength of the Pauli repulsion between the oxygen  $2p$  states and the metal  $d$  states.

lence states are sufficiently high-lying that the coupling to the  $d$  states is strong enough to push antibonding states above the Fermi level for gold. This is not possible for silver, which has a deeper-lying  $d$  band and a smaller coupling matrix element. For these adsorbates, silver is slightly more noble than gold.

Examination of the values of  $V_{ad}^2$  for the metals to the right for copper, silver, and gold in the periodic table (Fig. 10) shows that the smallest value is for zinc. These metals also have low-energy  $d$  states and no bonding contribution due to the emptying of antibonding states, and the strength of the oxygen bonding should therefore also be given primarily by the size of  $V_{ad}^2$ . The previously discussed scenario would therefore suggest that oxygen and the other electronegative adsorbates should bind most strongly to zinc and that after gold, mercury should be the most noble.

The transition metals to the left of copper, silver, and gold will have the repulsive Pauli repulsion in addition to the attractive interaction due to the empty antibonding states disucssed previously. Both the Pauli repulsion and the attractive interaction due to bond formation become stronger as the matrix elements become larger. As long as the repulsion is stronger than the attraction, the  $5d$  metals will be more noble than the  $4d$  metals, which will be more noble than the  $3d$  metals just above them in the periodic table. This reflects the fact that the  $5d$  orbitals are always more extended than the  $4d$  orbitals, which are in turn more extended than the  $3d$  orbitals (Fig. 10). Since the bond strength increases as a result of moving to the left and up in the transition metal series, the platinum group metals in the lower right corner should be the most noble.

## B. MOLECULAR ADSORBATES

The adsorption of molecules is only slightly more complicated to describe than atomic adsorption. The main complication arises from the fact that usually several adsorbate valence states are important for the interaction with a surface.

As the first example, consider the adsorption of CO. Several theoretical studies (51–54) suggest that the filled  $5\sigma$  and the doubly degenerate, empty  $2\pi^*$  electronic states are mainly responsible for the bonding to metal surfaces.

It is possible to understand the changes in electronic structure during CO chemisorption using exactly the same two-step process as for the atomic adsorbates. This is illustrated in Fig. 12. We consider here the change in the adsorbate density of states when a CO molecule interacts with a metal with only  $s$  electrons and the case in which there are also  $d$  electrons with which the CO states can interact. It is seen that the interaction with the metallic  $s$  electrons gives rise to a downshift and broadening of both the  $2\pi$  and  $5\sigma$  states, whereas the coupling to the metallic  $d$  states gives rise

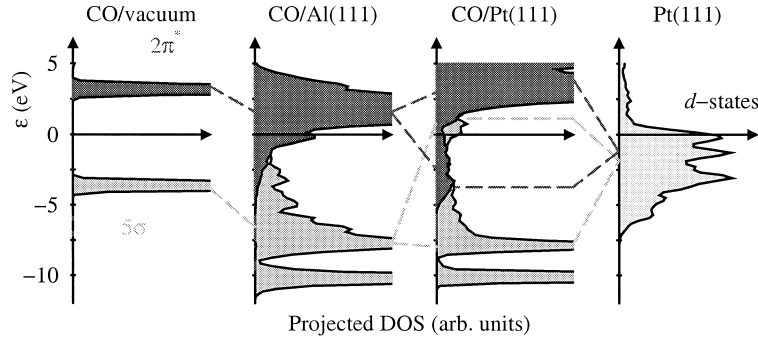


FIG. 12. The self-consistent electronic DOS projected onto the  $5\sigma$  and  $2\pi^*$  orbitals of CO: in vacuum and on Al(111) and Pt(111) surfaces. Also shown is the DOS from the  $d$  bands in the Pt(111) surface. The sharp states of CO in vacuum are seen to broaden into resonances and shift down in energy on the simple metal surface (mixing with the  $4\sigma$  state causes additional structure in the  $5\sigma$  resonance). On the transition metal surfaces the CO resonances further hybridize with the metal  $d$  states. This leads to shifts in the  $5\sigma$  and  $2\pi^*$  levels and to antibonding  $5\sigma-d$  states at the top of the  $d$  bands and bonding  $2\pi^*-d$  states at the bottom. These states have low weight in the  $5\sigma$  and  $2\pi^*$  projections shown. Adapted from Hammer *et al.* (55).

to bonding and antibonding states below and above the two original states. As a consequence of the different symmetries, the  $2\pi$  and  $5\sigma$  states interact with different  $d$  orbitals, and the two interactions can be treated independently.

The current model of CO bonding is in complete agreement with the theoretical interpretations developed by Blyholder (53), Bagus and Pacchioni (52), and Van Santen and Neurock (54). Usually, the CO–metal bond is described in terms of electron donation from the CO  $5\sigma$  to the metal and back-donation from the metal to the CO  $2\pi^*$ . With the current division of the donation and back-donation into separate metal  $s$  and  $d$  steps, which follows the reasoning of Bagus and Pacchioni (52), we obtain a simple picture that can even be developed into a quantitative model of the trends in the CO chemisorption energies on metal surfaces and overlayers (55).

Two important effects can be observed immediately from Fig. 12. First, the  $5\sigma$  contribution to the bonding is quite small. There are few antibonding states shifted above the Fermi level, and if we include the Pauli repulsion this interaction with the metal  $d$  electrons is repulsive (54). This is true for transition metals to the right in the periodic table and for copper, silver, and gold. The  $2\pi$  interaction, on the other hand, is attractive and dominates the variations from one metal to the next to the right in the periodic table. The large difference from the  $5\sigma$  case is that the  $2\pi$  state is above the Fermi level before interaction with the  $d$  states, and in this case new bonding states are shifted below the Fermi level. Note that there is an attractive

$2\pi$ -metal  $d$  interaction even for the noble metals. As we move to the left in the periodic table from the noble metals, the bond strength increases, again mainly because the  $d$  states move up in energy. The effect is considerably weaker than for the atomic adsorbates, however. This point is illustrated in Fig. 13, in which the calculated adsorption strength for adsorbed CO is compared with that of adsorbed carbon atoms and adsorbed oxygen atoms on some 4d transition metals. The molecular adsorption is strongest to the right, but farther to the left there is a crossover, and the dissociated state becomes the most stable. This type of behavior is quite general. In Fig. 13, a similar comparison for NO and adsorbed N + O is shown. The situation is the same, except that the crossover is farther to the right (56). For each of the simple molecular adsorbates there is such a crossover between atomic and molecular adsorption somewhere in the group of transition metals, as illustrated by the experimental results collected by Broden

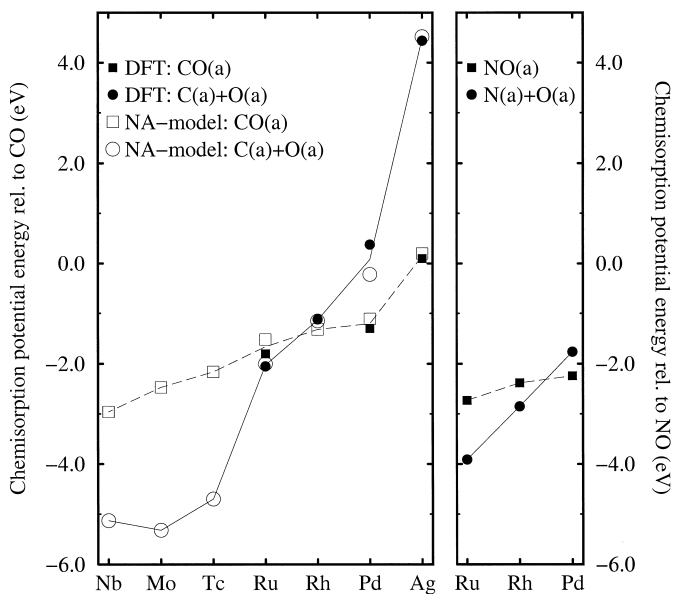


FIG. 13. (Left) Calculated (PW91) and model estimates of the variation in the adsorption energy of molecular CO compared to atomically adsorbed C and O for the most close-packed surface of the 4d transition metals. (Right) Calculated (PW91) molecular and dissociative chemisorption of NO. Solid symbols are DFT calculations; open symbols are Newns–Anderson model calculations. For CO, dissociative chemisorption appears to the left of rhodium. For NO, dissociative chemisorption appears farther to the right, i.e., also on rhodium.

*et al.* (57) (Fig. 14). The crossover point depends on the transition metal row—the 5d's tend to cause molecular dissociation less willingly than the 4d's and 3d's. The origin of this effect is the increase in nobleness from the 3d's to the 4d's and 5d's discussed previously. The crossover also depends on the molecule adsorbed, as reflected largely by the variations in atomic adsorption energies.

The above description of the bonding of molecules to surfaces is readily extended to even larger and more complicated molecules (58, 59). In Fig. 15, the analysis of Pallassana and Neurock (58) of the interaction between ethylene and a Pt(111) surface is shown.

### C. ADSORBATE-ADSORBATE INTERACTIONS

So far, we have mostly considered trends in adsorption energies for a fixed surface coverage. The surface coverage of reactants, intermediates, and products on a catalyst can vary significantly depending on reaction

CO	Sc	Ti D	V	Cr	Mn	Fe D	Co	Ni M	Cu
	Y	Zr	Nb	Mo D	Tc	Ru M	Rh	Pd M	Ag
	La	Hf	Ta	W D+M	Re	Os	Ir M	Pt M	Au
$N_2$	Sc	Ti (D)	V	Cr (D)	Mn	Fe D	Co	Ni	Cu
	Y	Zr	Nb	Mo (D)	Tc	Ru	Rh	Pd	Ag
	La	Hf	Ta	W (D)	Re	Os	Ir	Pt	Au
NO	Sc	Ti	V	Cr	Mn	Fe	Co	Ni D+M	Cu
	Y	Zr	Nb	Mo	Tc	Ru M	Rh	Pd M	Ag
	La	Hf	Ta	W	Re	Os	Ir D+M	Pt M	Au

FIG. 14. Compilation of experimental data for the ability of transition metals to adsorb and dissociate CO,  $N_2$ , and NO molecules. M, molecular adsorption; D, dissociative adsorption. Adapted from Broden *et al.* (57).

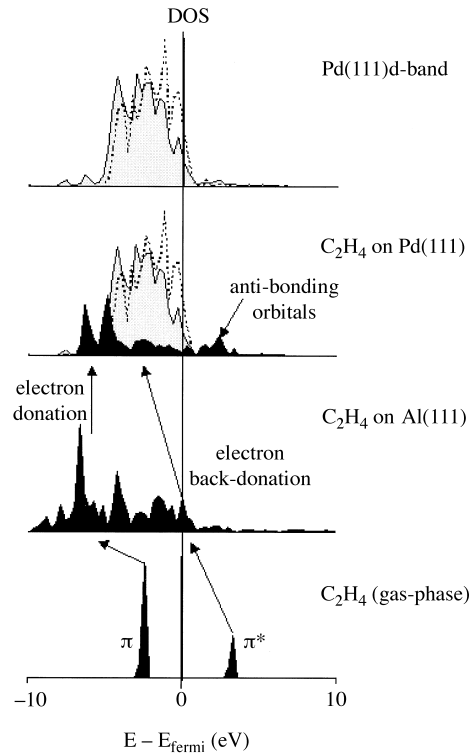


FIG. 15. Illustration of the interaction between C<sub>2</sub>H<sub>4</sub> and a Pd(111) surface. From Pallassana and Neurock (58).

conditions, and often the coverages are so large that adsorbate–adsorbate interactions are significant and should be included in the description. In fact, these interactions are often so large that a variation in the coverage can change the state of the surface more than the variation from one metal to the next in the periodic table.

As an example of a calculated coverage dependence, consider in Fig. 16 the nitrogen adsorption energy as a function of nitrogen atom coverage on various iron surfaces (60). The results illustrate that interactions can be both attractive and repulsive. The former leads to island formation at low coverages (and temperatures); even at relatively low coverages, adsorbates prefer to cluster together to take advantage of the attractive interaction. Such effects have been observed for the N/Fe(100) system (61), as suggested by the results shown in Fig. 16. Repulsive interactions do not lead to island formation but instead to dispersed overlayers and a strongly coverage-

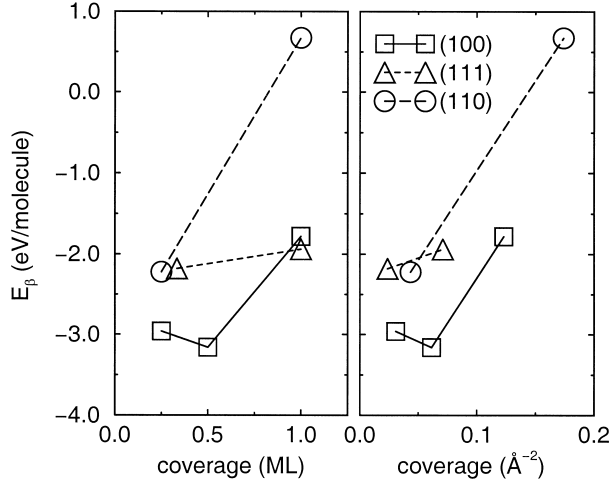


FIG. 16. Adsorption energies (PW91) for dissociated  $\text{N}_2$  on bcc-iron as a function of coverage. The squares correspond to  $(1 \times 1)$ ,  $c(2 \times 2)$ , and  $(2 \times 2)$ - $\text{N}/\text{Fe}(100)$  structures; the triangles represent  $(1 \times 1)$  and  $(\sqrt{3} \times \sqrt{3})\text{R}30^\circ$ - $\text{N}/\text{Fe}(111)$  structures; and the circles represent  $(1 \times 1)$  and  $(2 \times 2)$ - $\text{N}/(110)$  structures. From Mortensen *et al.* (60).

dependent heat of adsorption. Although attractive interactions are often quite weak and depend on the details of the system, repulsive interactions are very common, particularly at high coverages (62–64). They are often observed experimentally as a strong decrease in the heat of adsorption with coverage, as for example in the calorimetric results reported by Brown *et al.* (34) (Fig. 17).

The attractive interactions are usually dependent on details in the electronic structure. Attraction may also be a result of reconstructions of the surface. Consider for example the  $\text{N}/\text{Fe}$  system of Fig. 16. It is evident that the nitrogen atoms strongly prefer the local geometry provided by the  $\text{Fe}(100)$  surface relative to the two other low-index surfaces. The nitrogen atoms may therefore prefer to completely restructure the  $(110)$  or  $(111)$  surfaces to obtain a similar local geometry. For such a major restructuring to occur, an island of a certain size is needed in order for the reconstruction to be stable, and the result may be an effective attractive interaction between the nitrogen atoms mediated by the reconstruction on these surfaces, even though the intrinsic  $\text{N}-\text{N}$  interaction is strongly repulsive.

There are four common causes for interactions between like adsorbates:

1. Direct interactions due to overlap of wavefunctions: Direct overlap between adsorbate states may lead to attraction if there are states close

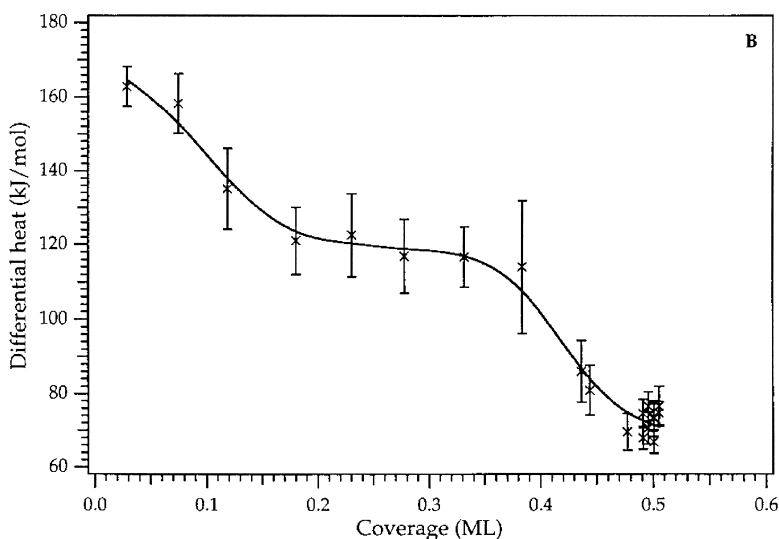


FIG. 17. The measured differential heat of adsorption of NO on Pd(100) as a function of coverage. Reprinted with permission from Brown *et al.* (34) © 1998 American Chemical Society.

enough to the Fermi level that the interaction can shift states through the Fermi level. This is often not the case, and the interaction is then dominated by the Pauli repulsion. The detailed analysis of O–O interactions on a Pt(100) surface by Ge and King (65) illustrates this effect in detail (Fig. 18).

2. Indirect interactions: One adsorbate may change the electronic structure of the surface in such a way that the adsorption energy of a second adsorbate is changed. One commonly observed effect is that adsorption leads to a downshift of the *d* states of the neighboring transition metal atoms (47, 66). As shown previously, a downshift of the *d* states usually leads to a weaker interaction with an adsorbate. This means that a second adsorbate trying to bond to the same transition metal atoms as the first may be bound less strongly. This effect is discussed later.

3. Elastic interactions: Adsorption usually leads to local distortions of the surface lattice. This distortion is experienced by other adsorbates as a repulsion (67, 68).

4. Nonlocal electrostatic effects: These can, to lowest order, be described as dipole–dipole interactions.

In addition to interactions with other adsorbates of the same kind, interactions with other kinds of adsorbates may also be important. We return to

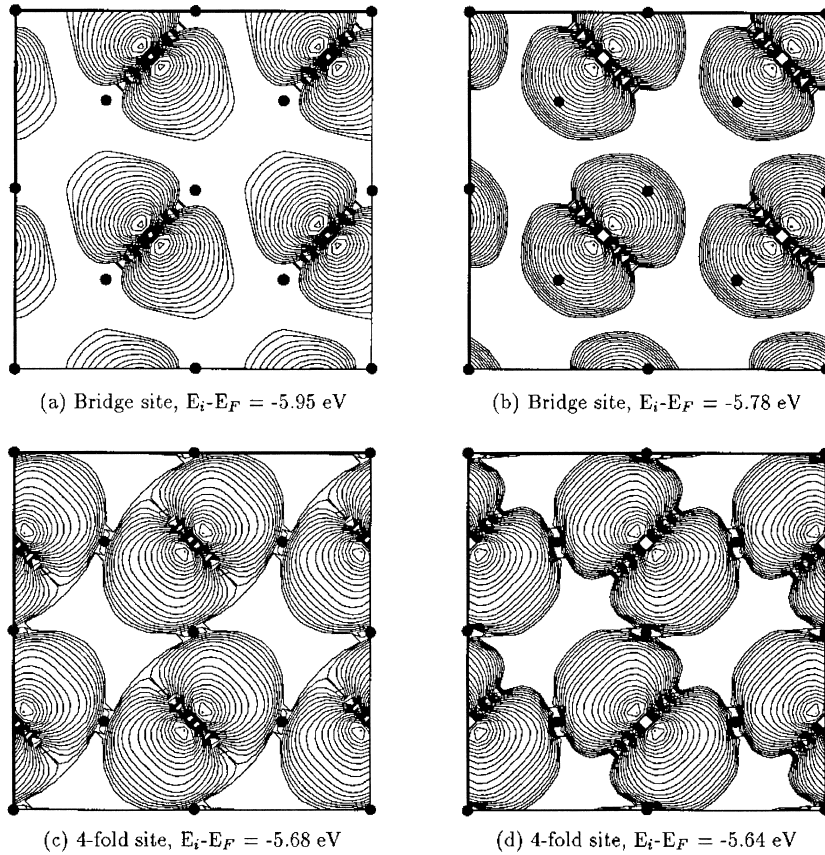


FIG. 18. Charge density contours for oxygen-induced states 5 or 6 eV below the Fermi level on Pt(100). For adsorption in the fourfold sites, in which the O–O repulsion is large, the oxygen p-like states are seen to overlap substantially more than for oxygen atoms in the twofold sites, in which the repulsion is weaker. From Ge *et al.* (65).

this topic in connection with our discussion of poisoning and promotion in Section V.C.

The strong coverage dependence of adsorption energies profoundly affects the reactivity of a surface. A more weakly bound adsorbate may be more reactive, and changing the reaction conditions (temperature and/or partial pressures) can therefore change the reactivity considerably. This has recently been exploited by Bradley *et al.* (69) to suggest new reaction conditions for the ammonia oxidation on platinum catalysts.

#### IV. Bond-Making and -Breaking at a Surface

We now discuss the question of how to describe reactions at surfaces. Any chemical reaction can be described as a transition between two local minima on the potential energy surface of the system as a function of the coordinates of all the involved atoms. The reaction path we define as the minimum energy path leading from the reactant minimum to the product minimum. The saddle point on this path defines the transition state, and the energy difference between the saddle point and the reactant minimum is the activation energy ( $E_a$ ) of an elementary process. Figure 19 illustrates a potential energy surface in two important degrees of freedom for a dissociative adsorption process (or, equivalently, a recombinative desorption process). Figure 19 also shows the minimum energy path as well as the usual one-dimensional representation of such a reaction, in which the energy is shown as a function of the distance along the reaction path (the reaction coordinate). We stress that in general there are not just a few degrees of freedom taking part in the reaction. Usually, several of the adsorbate degrees of freedom are important, and there are cases for which deformation of the surface is also an important part of the reaction (47, 70).

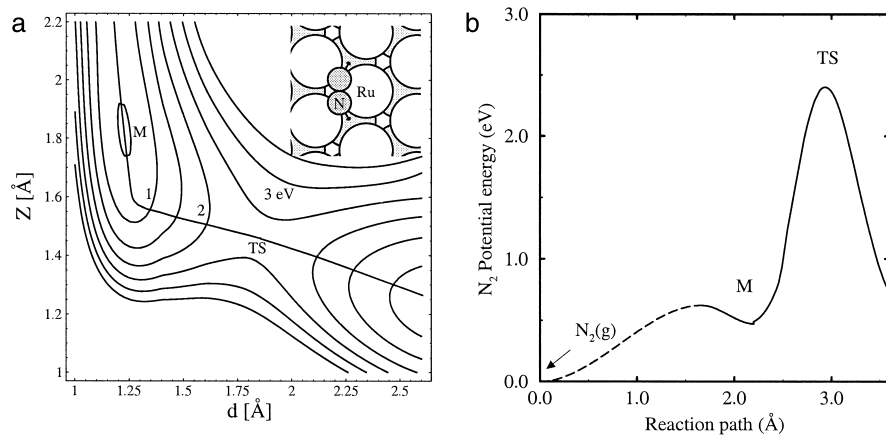


FIG. 19. (a) The potential energy surface (RPBE) for  $\text{N}_2$  dissociating on a Ru(0001) surface. The energy zero is a molecule far from the surface. The adsorption geometry is shown in the inset. The distance of the center of mass of the molecule above the surface,  $Z$ , and the N–N bond length,  $d$ , are varied. The minimum energy path is indicated, and in (b) the energy along the path is shown. Note that here only two degrees of freedom have been included. When the rest are included, the minimum energy path has a lower energy barrier (Fig. 34). Adapted from Murphy *et al.* (71).

The rate of an elementary step is given in general by an Arrhenius expression such as

$$r = \nu e^{-E_a/kT}, \quad (1)$$

where  $E_a$  is the activation energy,  $k$  is Boltzmann's constant, and  $T$  is the temperature. The prefactor  $\nu$  is also given by the properties of the potential energy surface. We do not discuss this aspect but refer, for example, to the review by Van Santen and Neurock (54). We also note that the modeling of particular experiments, e.g., molecular beam and state-resolved desorption studies, may require that the *dynamics* of a surface reaction be considered. For a further discussion of this topic, see recent reviews by Darling and Holloway (72), Groß (73), and Kroes (74). In the following sections, we concentrate on the factors controlling the activation energy. We show that trends in activation energies can be understood by using the same concepts developed previously to understand atomic and molecular adsorption energies.

#### A. THE REACTION PATH AND THE NATURE OF THE TRANSITION STATE

In Fig. 20, the transition states of some elementary reaction steps on close-packed surface of transition metals are shown. Two types of reaction

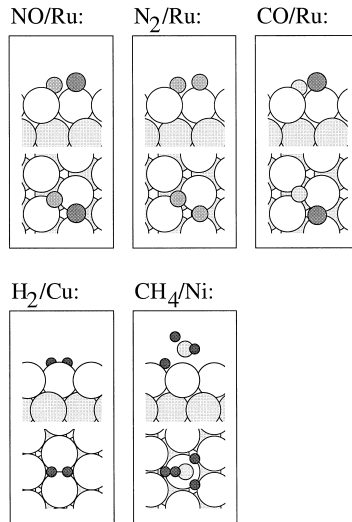


FIG. 20. Transition states for some dissociation reactions of small molecules on transition metal surfaces. The geometries are taken from Hammer (84) (NO/Ru), Dahl *et al.* (83) ( $N_2$ /Ru), Mavrikakis *et al.* (14) (CO/Ru), Hammer *et al.* (32) ( $H_2$ /Cu), and Kratzer *et al.* (86) ( $CH_4$ /Ni).

paths can be observed. For the dissociation of diatomics such as CO, NO, and N<sub>2</sub>, the transition state is a highly stretched molecule (75–78). One of the atoms is already close to the final, threefold-coordinated site, whereas the other is on its way to the nearest similar (fcc or hcp) site. At the transition state it is more or less in a twofold coordination site corresponding to the top of the barrier for diffusion of one of the atoms. The same is true for the transition state of, e.g., the CO + O reaction (or, equivalently, the CO<sub>2</sub> dissociation) (79–81) and for C–C bond breaking or formation (82).

The other type of path shown in Fig. 20 is one in which the transition state is much less stretched. This type of reaction is characterized by an initial state with a very short bond (typically involving hydrogen), and the stretched transition state observed for the “longer bonds” is well beyond the point at which the bond is broken.

The electronic structure at the transition state reflects the two different kinds of reaction paths. For “short” transition states, such as for H<sub>2</sub> dissociation, the transition state has bonding and antibonding states, as in the molecule (Fig. 21). Clearly, the interaction of these states with the surface electrons can be thought of in the same way as for the atomic and molecular adsorbates. The coupling to the metal *s* electrons gives rise to a broadening, and the coupling to the transition metal *d* electrons gives rise to bonding and antibonding states. Just as for CO adsorption, the adsorbate states of different symmetry (the bonding  $\sigma_g$  and the antibonding  $\sigma_u^*$  H<sub>2</sub> states) can be treated independently.

For the “stretched” transition states, the electronic structure of the transition state is much more like that of the adsorbed atoms than that of the

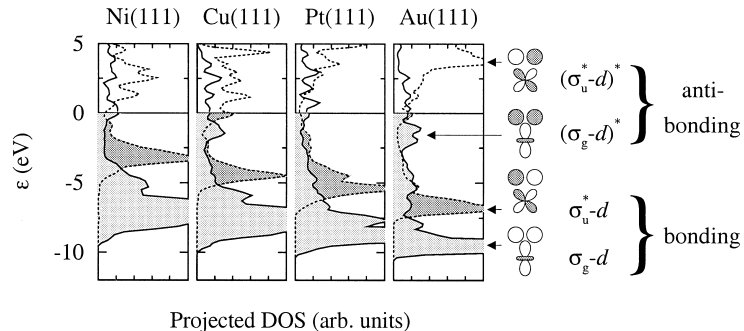


FIG. 21. The DOS projected onto  $\sigma_g$  and  $\sigma_u^*$  for H<sub>2</sub> in the dissociation transition state on Cu(111), Ni(111), and Au(111), and Pt(111) surfaces. From Hammer and Nørskov (40).

adsorbed molecule. This is illustrated in Fig. 22, in which the density of states projected onto the two nitrogen atoms in the transition state for  $N_2$  dissociation on Ru(0001) is shown. Because of the highly stretched N–N bond length in the transition state (1.9 Å), the electronic structure of the molecule is very final state-like. The distinct splitting of the nitrogen 2p states into  $2\sigma_u$ ,  $1\pi_v$ ,  $3\sigma_g$ , and  $1\pi_g$  molecular-like states for adsorbed  $N_2$  (not shown) is thus disappeared in the transition state.

### B. VARIATIONS IN REACTIVITY FROM ONE METAL TO THE NEXT

Since the electronic structure is understandable in the same language as that developed to describe atomic and molecular adsorption, the variation in the energy of the transition states—or, equivalently, the activation barriers—follows along the same lines.

Consider as the first example the  $H_2$  dissociation on copper, nickel, gold, and platinum. The energy along the reaction path is shown in Fig. 23. In agreement with experimental knowledge, nickel and platinum each has a low barrier and dissociates  $H_2$  readily (87, 88), whereas copper has a sizable barrier (89) and  $H_2$  dissociation is impossible on gold (90). Just as for the adsorption cases discussed previously, there are two effects involved. Nickel and platinum are more reactive than copper and gold, mostly because more bonding states between the initially empty antibonding  $H_2$  state and the metal  $d$  states are shifted below the Fermi level. Again, the general rule is that the higher the  $d$  band center, the more reactive the metal (that is, the lower the transition state energy) (46, 45, 91).

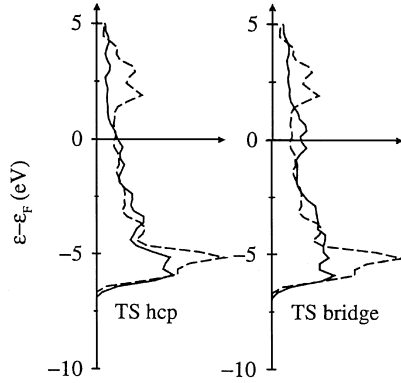


FIG. 22. DOS projected onto 2p orbitals of the two nitrogen atoms in the transition states for  $N_2$  dissociation on Ru(0001). One atom is close to an hcp site and one close to a bridge site. Both DOS are compared with the DOS projected onto the 2p orbitals of a nitrogen atom adsorbed at an hcp site (dashed lines). From Mortenson *et al.* (47).

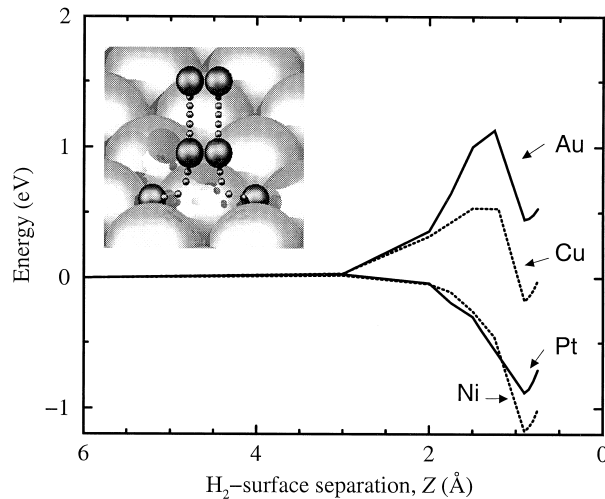


FIG. 23. The potential energy (PW91) along the atop reaction path for  $\text{H}_2$  dissociating on copper, nickel, gold, and platinum.  $Z$  is the  $\text{H}_2$  height above the plane of the surface atomic position. From Hammer and Nørskov (46). Reprinted by permission from *Nature* (46) © 1995 Macmillan Magazines Ltd.

Gold (and to a lesser extend platinum) is less reactive than copper (or nickel) because the Pauli repulsion is larger for the  $5d$  metals than for the  $3d$  metals, just as discussed previously for atomic adsorbates. The dissociation of  $\text{H}_2$  on rhodium, palladium, silver, and tungsten surfaces has been investigated with DFT methods, with the results being consistent with the current picture (91–95).

The picture is even simpler for the stretched transition states. Since they are very final state-like, the variations in the transition state energies closely follow the variations in the adsorption energies of the products, as illustrated in Fig. 24.

The strong coupling between transition state energies and final state energies has as an important consequence, namely, that the search for the perfect transition metal to catalyze a certain reaction is always a compromise. Moving to the left in the transition metal series gives a lower activation energy but also stronger bonding of the reactants and thus less free surface area. The “Sabatier principle”-type behavior usually leads to “volcano curves” describing the relation between catalytic activity and position in the periodic table (2).

For the “late” barrier processes, the transition state energy is considerably higher than the final state energy for two reasons: (i) In the transition state, one of the atoms is in the twofold site, which is higher in energy than

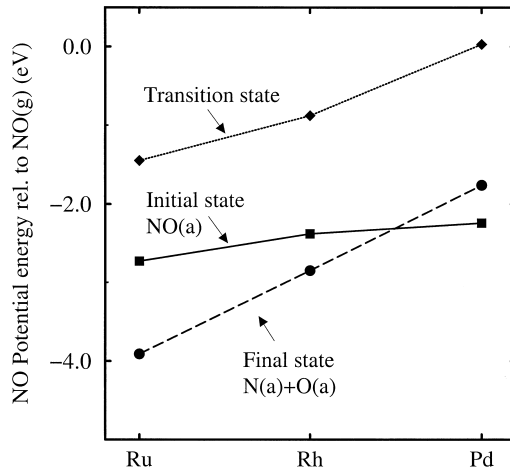


FIG. 24. The variation in energy (PW91) of the initial, transition, and final state for NO adsorption on the tcc(111) surfaces of the 4d transition metals Ru, Rh, and Pd. The correlation between the transition and final state energies is clearly evident. Data from Mavrikakis *et al.* (75) and Hammer (84, 110).

the equilibrium threefold site, and (ii) the two dissociating atoms share two surface metal atoms in the transition state, giving rise to a large repulsion.

## V. Changing the Reactivity

In the preceding sections, we discussed variations in the stability of adsorbed atoms and molecules or of the transition state complex for surface chemical reactions from one metal to the next. Here, we focus on even more subtle variations in reactivity. Often, the reactivity of a given metal can be changed substantially by changing the surface structure, by alloying, or by introducing additional adsorbates onto the surface. In the following sections, we discuss each of these cases separately and show that the underlying mechanisms responsible for the variations in reactivity are the same.

### A. STRUCTURE SENSITIVITY

The chemisorption and reaction properties of a metal surface depend on the electronic as well as the geometric structures of the surface. Although the electronic and geometric structures of a surface usually cannot be varied independently, it is very useful to consider the two as causing independent effects on the reactivity of a surface. The two effects are usually termed

“electronic” and “geometric” effects. The electronic effects originate from the local electronic structure of the surface and are given by the one-electron spectrum of the metal states that interact with the adsorbates. In most cases, in continuation of the previous discussion, the local average of the  $d$  electron energies,  $\varepsilon_d$ , suffices to describe the electronic effect.

The geometric effect is “the rest,” so to speak. If adsorbates or reaction complexes interact in different geometric arrangements with surface atoms with identical local electronic properties, the differences in chemisorption bonds and energy barrier heights are ascribed to the differences in the bonding geometry. The simplest measure of the geometric effect is thus the coordination number of the adsorbate with respect to the surface atoms.

### 1. Strain

We start by considering a transition metal surface subject to strain. The geometric arrangement of the surface atoms changes only slightly when the interatomic distances parallel to the surface are modified. Threefold adsorption sites, for example, are still threefold adsorption sites (only the bond lengths have changed), and an adsorbate may compensate for this change by relaxing in the direction perpendicular to the surface. Studying surface processes as a function of strain therefore offers a means of evaluating the magnitude of the electronic effect.

When a surface undergoes compressive or tensile strain, the overlap of metal  $d$  states at neighboring sites will either increase or decrease and so will the  $d$  bandwidths. It is a general finding of our density functional calculations that no charging or discharging of the  $d$  states of late transition metal sites follows from a change in  $d$  bandwidth. Rather, the  $d$  bands move in energy to maintain a constant filling. Compressive or tensile strain therefore leads to downshifts and upshifts of the  $d$  band centers, respectively. The effect is illustrated in Fig. 25.

Figure 26 illustrates two ways in which strained surfaces can be realized experimentally in connection with single-crystal surfaces. Gsell *et al.* (96) modified a ruthenium surface through ion implantation by a noble gas. This treatment causes regions of the surface to buckle out. The middle of these regions is subject to tensile strain, whereas the periphery of the regions is subject to compressive strain. Another experimental possibility involves evaporation of one metal onto another (97–102). By choosing combinations of metals that give pseudomorphic growth of a monolayer of one metal on the other, highly strained surfaces of the one metal can be realized. Both of these strained metals are easily modeled by DFT calculations—either as slabs under uniform lateral strain or as “sandwich slabs” of one metal on another with the surface unit cell area determined by the substrate

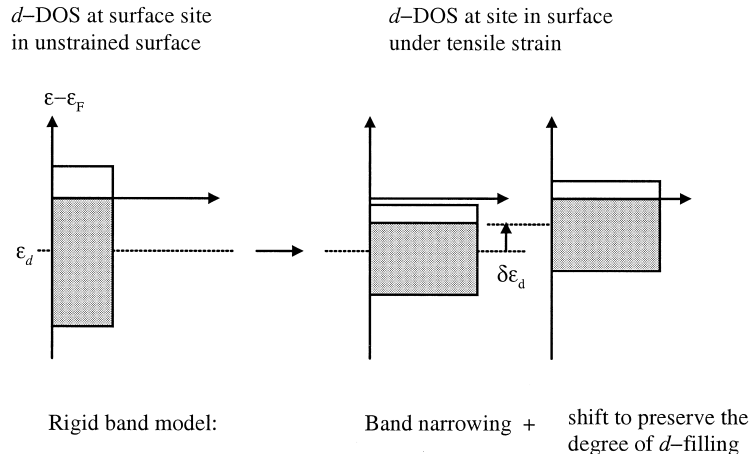


FIG. 25. Illustration of the effect of tensile strain on the  $d$  band center. Increasing the lattice constant shrinks the band width, and, to keep the number of  $d$  electrons fixed, the  $d$  states have to move up in energy.

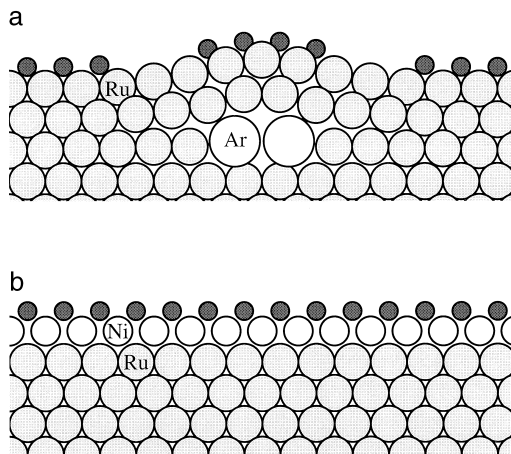


FIG. 26. Two ways of inducing strain on a single-crystal surface: (a) by Ar bubbles; (b) by the growth of strained pseudomorphic overlayers. Dark circles indicate adsorbates bound in regions of tensile strain.

metal. A third possibility involves characterization of dislocations ending at the surface (103).

Figure 27 shows the DFT results for adsorption and dissociation of CO on strained Ru(0001). The chemisorption potential energies and reaction energy barriers are plotted versus the  $d$  band center. A clear correlation between the chemisorption energies or energy barriers and the  $d$  band center is established. This correlation can be understood by comparison with the model calculation in Fig. 4. Here it was found that the higher the energy of the  $d$  bands, the more likely antibonding metal  $d$  adsorbate states are to be pushed above the Fermi level and the more likely the metal  $d$ -adsorbate interaction is to become net attractive.

The strain effect is not limited to CO adsorption and dissociation on ruthenium. Figure 28 shows the activation energy for  $N_2$  dissociation on hexagonally close-packed iron surfaces with different lattice constants. Again, large lattice constants with high-lying  $d$  states are the most reactive.

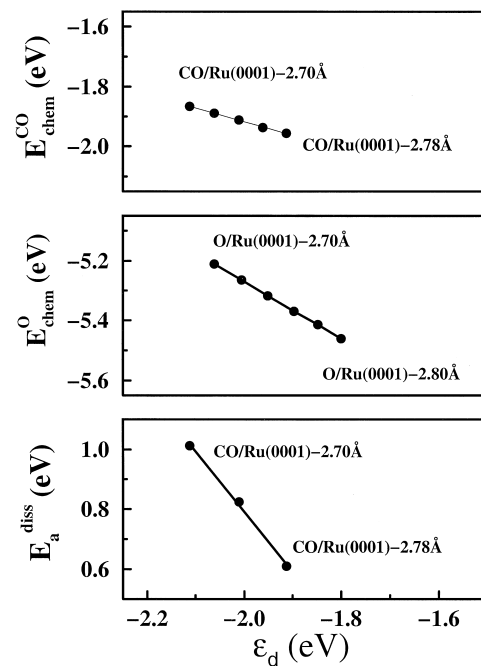


FIG. 27. Calculated (PW91) variation in the adsorption energy of CO, the adsorption energy of atomic oxygen, and the energy barriers for CO dissociation on a Ru(0001) surface for different lattice constants. The variations in energy are shown to be correlated with the variations in the  $d$  band center  $\varepsilon_d$ . Adapted from Mavrikakis *et al.* (14).

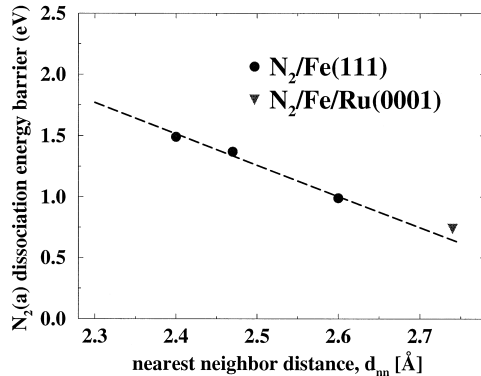


FIG. 28. Variation in the energy barrier for  $N_2$  dissociation on a close-packed fcc–Fe(111) surface as a function of the nearest-neighbor separation in the surface. Also included is the result for a single layer of iron on Ru(0001). This point is placed at the equivalent ruthenium nearest-neighbor separation. The fact that it falls in line with the other points suggests that the main effect of the ruthenium substrate is to stretch the iron overlayer. From Logadottir (104).

Furthermore, one point corresponding to a monolayer of iron on Ru(0001) is included. It can be seen that the effect is the same and that the Fe/Ru(0001) point falls in line with the general trends. This result shows that in this case the main effect of the ruthenium is to increase the iron lattice constant. One would get the same result even without the ruthenium underneath.

Additional examples are shown in Fig. 29. Here, results from Pallassana and Neurock (58) for the activation energy for dehydrogenation of ethylene and of ethyl on different palladium overlayers are shown. Palladium on gold is more reactive than pure palladium because the gold lattice constant is larger than the palladium lattice constant and vice versa for ruthenium. The palladium/rhenium result represents an exception to the general rule that the main effect of the substrate is to change the lattice constant of the overlayer. The two metals have essentially the same lattice constant, but the palladium overlayer is less reactive than pure palladium. We note, however, that the shift in  $\varepsilon_d$  does capture the correct trend. In this case, the shift must be caused primarily by the interaction between the electrons in the palladium overlayer and the rhenium atoms underneath. We therefore conclude this section by noting that the reactivity scales very well with shifts in  $\varepsilon_d$  for both strained crystals and overlayers.

For nanosized supported catalysts, not just overlayers of one metal on another can have a changed reactivity due to strain. Small metal particles on an oxide support may also have a lattice constant (and thus a reactivity)

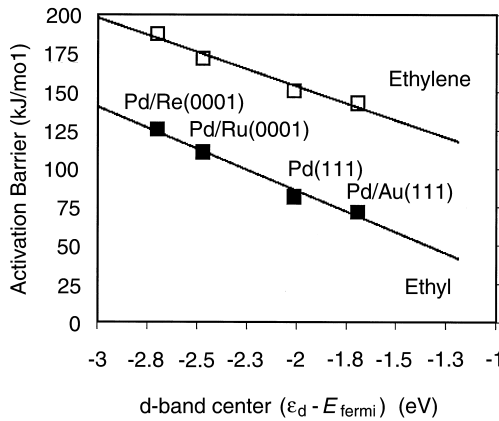


FIG. 29. Variations in the transition state energy for dehydrogenation of ethylene and of ethyl on Pd(111) and on palladium overlayers on various other metals. The variations in activation energy correlate well with the variations in the *d* band centers for the surface palladium atoms. From Pallassana and Neurock (58).

different from that of a large facet. Two factors play a role: (i) the surface tension and (ii) the interaction with the support. The former usually tends to decrease the lattice constant, whereas the latter may both increase and decrease the lattice constant. There are many examples in which lattice constants different from the bulk value have been observed for supported metal nanoparticles (105–107), and we expect this to be a very general phenomenon. Both the surface tension effect and the strain induced by the oxide support will be most important for very small particles, and the effect will decrease with increasing particle size.

## 2. Different Facets

When comparing the reactivities of different surface facets [e.g., fcc(111) and fcc(100)], both the electronic and the ion structure change. The change of the electronic structure is a consequence of the change of the ionic structure. We maintain, however, the strict division into electronic and geometric effects.

If an adsorption or reaction configuration is sufficiently simple, it is sometimes possible to disentangle the electronic and geometric effects, even when comparing different facets. Figure 30 shows examples of this: an atop bonding of CO on a range of platinum surfaces (108) and an H<sub>2</sub> transition state complex on two different copper surfaces (109). Because the local chemisorption configuration of CO is the same on all platinum

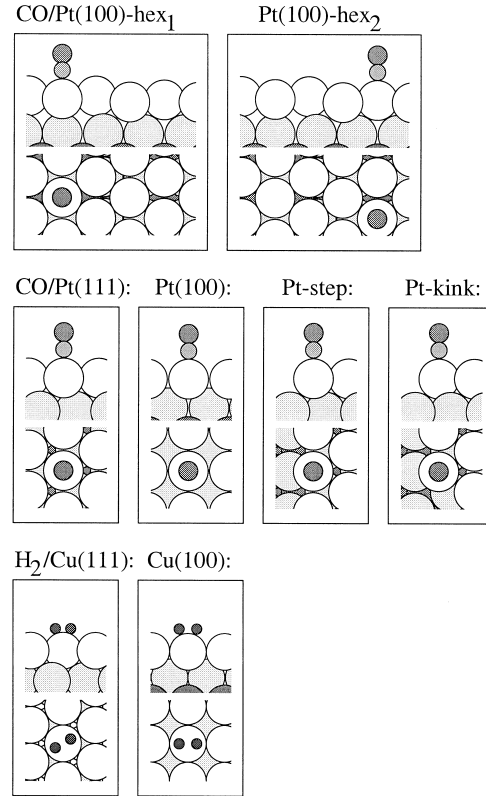


FIG. 30. Different ways of changing the adsorption or reaction geometry while not changing the local geometry. The chemisorbed CO and the H<sub>2</sub> transition state complex are probing the local electronic structure effects.

surfaces in Fig. 30, the variations in the CO chemisorption potential energy must be ascribed primarily to the electronic effects (although second-neighbor effects may also be of some importance). Likewise, because the H<sub>2</sub> reaction geometry (over the atop site into bridge sites) is the same on the two copper surfaces considered, the variations in the H<sub>2</sub> dissociation energy barriers must be ascribed to the changes in the electronic structure between the facets. The correlation of the CO chemisorption energy and H<sub>2</sub> dissociation energy barrier with our parameter for the electronic effect, the local center of the metal *d* states, is presented in Fig. 31, which shows that when the adsorption or reaction geometry is kept fixed, the effect of the facet is well described by the *d* band center.

The magnitude of the geometric effect can be estimated by allowing the

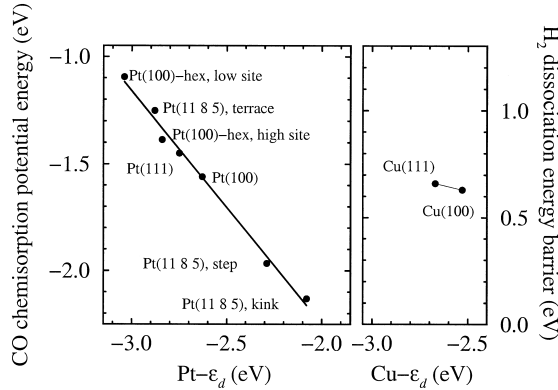


FIG. 31. (Left) Calculated variations in the chemisorption energy (PW91) for CO adsorbed atop platinum atoms in different surroundings. (Right) DFT energy barriers (PW91) for dissociative adsorption of  $H_2$  atop copper atoms in two different copper surfaces. The correlation between chemisorption energy and the  $d$  band center for the relevant platinum atoms is evident. Adapted from Hammer *et al.* (108) and Kratzer *et al.* (109).

adsorbate or transition state complex to exploit all available ionic degrees of freedom in the bond formation rather than restricting the geometry as was done previously. For the  $H_2$  dissociation, new optimum transition state complexes result on the different copper surfaces. These are shown in Fig. 32. On  $Cu(100)$ , a tilted configuration of the  $H_2$  transition state complex is found in which a hydrogen atom is almost in a fourfold hollow site (33). On  $Cu(111)$ , the  $H_2$  axis is parallel to the surface and both hydrogen atoms are in threefold-like positions. The transition state potential energies are reduced by 0.14 and 0.03 eV for  $Cu(111)$  and  $Cu(100)$ , respectively, com-

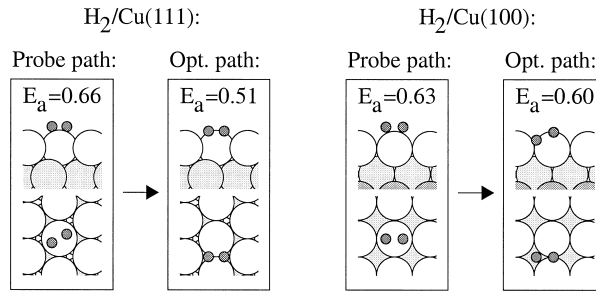


FIG. 32. The calculated transition states and (PW91) energy barriers (in eV) for  $H_2$  dissociation on  $Cu(100)$  and  $Cu(111)$ . Both the transition state for the atop path used to probe the electronic effect and the optimum energy path are shown. Adapted from Kratzer *et al.* (109).

pared with the values obtained by using the restricted transition state configurations of Fig. 30. The difference, 0.11 eV, is thus a measure of the geometric effect for H<sub>2</sub> dissociation on a low-index copper surface.

### 3. Steps and Defects

When considering high-Miller-index surfaces with steps and kinks, or surfaces with other defects such as adatoms or vacancies, the variations in the electronic structure become larger (i.e.,  $\varepsilon_d$  varies more). Again, the smaller the metal coordination number of the surface atom, the smaller the *d* band width and hence the higher energy of the *d* band center (if the *d* band is more than half filled). The electronic effect is completely analogous to what we have previously demonstrated. This may be seen from Fig. 31, in which the CO bonding to step and kink platinum atoms is also included.

The electronic effect may become so large at the step edges of metal surfaces that it can change the site preference of atomic adsorbates. For example, on a flat Ru(0001) surface, an oxygen atom prefers threefold bonding at an hcp site by 0.54 eV over twofold bonding at a bridge site. On Ru(0001), all ruthenium atoms have the same *d* band center, and therefore the site preference is a purely geometrical effect, originating from the change in coupling matrix element, adsorbate coordination, and nonlocal electrostatic effects caused by the change in adsorption site. On a monoatomic step on Ru(0001), however, the oxygen is as stable (within the calculational accuracy) in a hang-off-the-edge, twofold bonding configuration at the step edge as at an hcp threefold site behind the step edge, and it is preferred in the hang-off-the-edge configuration over the fcc threefold configuration by 0.27 eV. The configurations are depicted in Fig. 33 (110). The reason for the change in site preference from threefold at Ru(0001) to twofold at a monoatomic step can (with our division) be ascribed to the electronic effect (i.e., the finding that at the step edge the lower coordination of the surface atoms leads to energetically higher *d* bands and hence to higher reactivity). Similar effects have been observed, for example, by Feibelman *et al.* (111) for the O/Pt(111) system.

The electronic effect at steps is quite general. In addition to the examples stated previously, it has been shown in calculations that steps increase the stability of NO, N, and O on palladium (38, 66) and of N<sub>2</sub> on platinum (112) and that they lower the barrier for CH<sub>4</sub> dissociation on nickel (113), increase the stability of various C<sub>2</sub>H<sub>x</sub> species on platinum, and lower the barriers for C–H and C–C bond breaking on the same surfaces (82).

The geometric effect, however, may also become more prominent at a step edge. This has been illustrated in two recent studies of activation of NO and N<sub>2</sub> at monoatomic steps on Ru(0001) (83, 84). It was found that

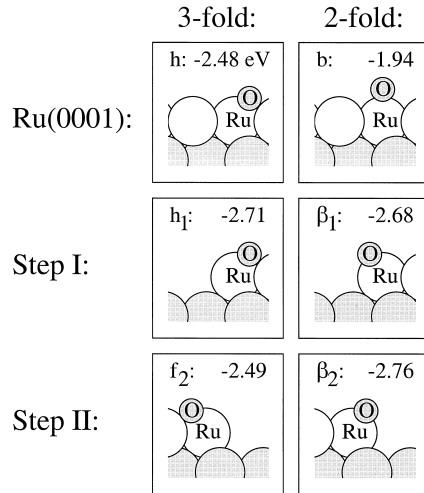


FIG. 33. Chemisorption of oxygen on a flat and stepped Ru(0001) surface. The chemisorption potential energy is given in eV. On the flat Ru(0001) surface threefold hcp chemisorption ( $h$ ) is highly preferred over twofold bridge chemisorption ( $b$ ). At the step edges, hcp chemisorption ( $h_1$ ) is comparable to bridge chemisorption ( $\beta_1$ ) for one-step geometry (step I), and bridge chemisorption ( $\beta_2$ ) even becomes preferred over fcc chemisorption ( $f_1$ ) at the other step geometry (step II). Adapted from Hammer (110).

the N–O and N–N bond activation barriers almost vanish for a reaction geometry in which the molecules initially are positioned at the base of the step. The effect is too large to be ascribed solely to the electronic effect at the step edge, the size of which is known from the NO and N<sub>2</sub> dissociation in configurations at the top of the step edges. Rather, a stabilization of the transition state complex on the order of 0.3 eV must be explained as originating from the geometric effect. In Fig. 34, the NO and N<sub>2</sub> transition state complexes are shown for reaction on flat and stepped Ru(0001), and the potential energy diagram is given for N<sub>2</sub>. The NO and N<sub>2</sub> are seen to coordinate to five ruthenium atoms in the highly reactive configurations at the base of the step edges, whereas they coordinate to only four ruthenium atoms on flat Ru(0001). The coordination to more ruthenium atoms at the step increases the total coupling matrix element between metal  $d$  states and adsorbate valence states. Simultaneously, the indirect repulsion between the reaction products (the chemisorbed nitrogen and oxygen atoms) is reduced (see Section III.C).

There is extensive experimental evidence that bonding is stronger at steps than at facets (2, 114, 115). The generality of the effect suggests that it may even be more important than has been realized. In the case of NO

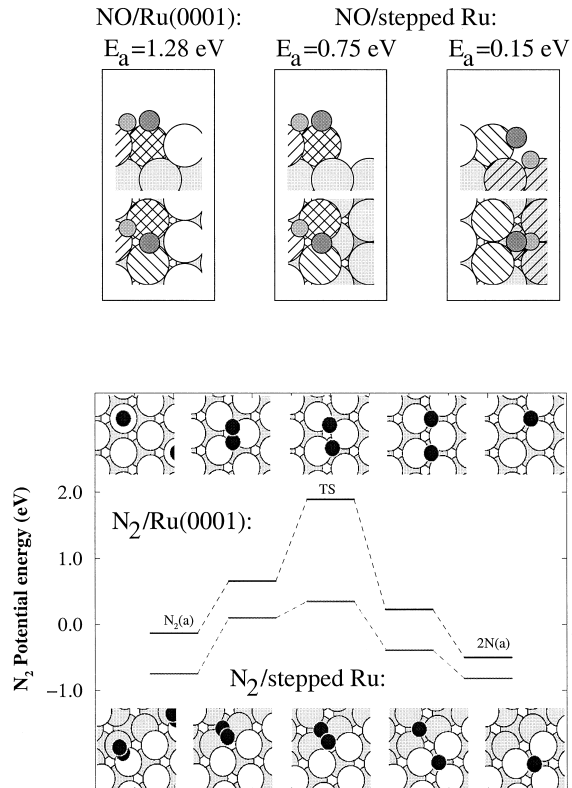


FIG. 34. (Top) Transition state geometries and corresponding energies (PW91) for NO dissociation on Ru(0001) terraces and steps. (Bottom) Reaction path and energies (RPBE) for  $\text{N}_2$  dissociation on the same surface. Again, both a terrace and a step configuration have been considered. In both cases the energy zero is the molecule far from the surface. Adapted from Dahl *et al.* (83) and Hammer (84).

dissociation on Ru(0001) steps, it has been shown by direct observation of the dissociation products by scanning tunneling microscopy that the dissociation occurs primarily at steps (116). In the case of  $\text{N}_2$  dissociation on Ru(0001), the reactivity of the steps is so much greater than that of the terraces that even the few steps present on any single-crystal surface (on the order of 1%) are enough to completely dominate the experiments. In this case, it was the large barrier found in the calculations that led to the discovery that the experiments were actually not measuring the reactivity of the terrace atoms (83, 117).

Traditionally, reactions in heterogeneous catalysis have been divided

into structure-sensitive and structure-insensitive reactions, depending on whether the reaction rate depends on particle size (118–120). A particle-size-dependent activity is usually a simple consequence of the structure dependence discussed previously. For small catalyst particles, the ratio of the different facets and the density of steps and other defects will be strongly dependent on particle size. Such structure sensitivity, however, may also be a consequence, for example, of the strain effect discussed in Section V.A.1.

### B. ALLOYING

Another way of changing the reactivity is through alloying. The addition of one or more chemical elements to a metallic surface increases the possible bonding geometries of adsorbates and reaction complexes and simultaneously changes the electronic structure of the alloy surface from that of the pure metallic surface alone. The effect of alloying may also be more indirect, however, if, for example, one of the alloy elements segregates to the surface. In this case, effects such as strain in the surface due to a difference in bulk lattice parameters of the alloy and its elemental components can be used to understand the effect of alloying (see Section V.A.1).

The reactivities of many alloy surfaces have been studied by density functional theory.  $H_2$  dissociation, which is nonactivated on Ni(111), was found to experience large energy barriers—even on nickel sites—on NiAl(110), and the increased repulsion can be assigned the electronic effect and traced to a downshift of the nickel  $d$  bands in the alloy (45, 121). Similarly, the platinum sites in a Cu<sub>3</sub>Pt(111) surface were found to be more reactive with respect to  $H_2$  bond activation than platinum sites in the Pt(111) surface, and again it is an electronic effect originating from an upshift of the platinum  $d$  bands on alloying (45).

An interesting type of alloy, Au/Ni, was investigated by Kratzer *et al.* (86) for its ability to dehydrogenate methane. Gold and nickel are immiscible in the bulk, but a two-dimensional (2-D) surface alloy exists in which gold alloys into the outermost layers of a Ni(111) crystal (Fig. 35). The alloy is interesting from a synthesis point of view because the gold does not dissolve into the nickel bulk, which implies that only small traces of gold are required to create the alloy (122, 123). The gold is inert for methane decomposition, and because the gold causes a downshift of the nickel  $d$  bands at neighboring sites, the ability of the alloy to catalyze the C–H bond activation is slightly inferior to that of the clean Ni(111) (Fig. 36). A nickel-based catalyst, however, suffers from carbon deposition (growth of carbon whiskers) during operation (124). Due to the electronic effect, carbon is found to bond less favorably to the Au/Ni(111) surface than to the Ni(111) surface. The inhibition of the carbon formation process is often more important than a

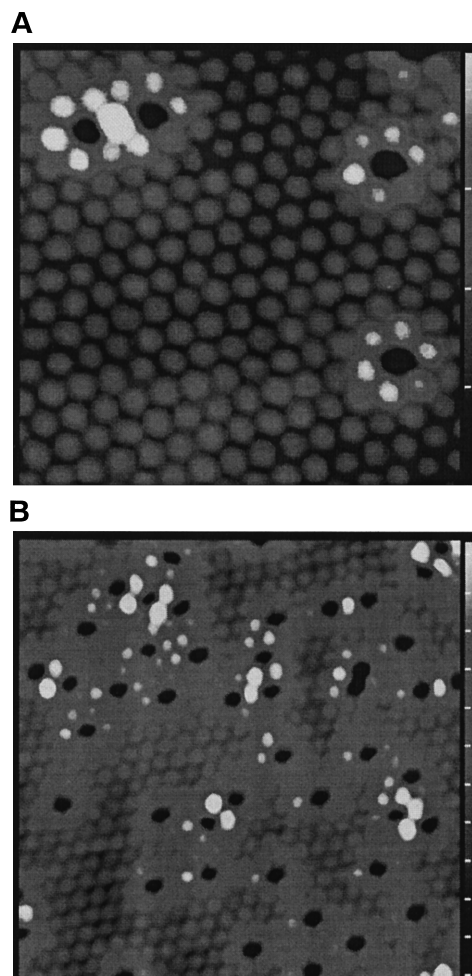


FIG. 35. Two STM images of a Ni(111) surface with 2% (A) and 7% (B) of a monolayer of gold. The gold atoms appear black in the images. The nickel atoms next to the gold atoms appear brighter due to a change in geometry and electronic structure, indicating that the chemical reactivity of the nickel atoms may be modified by nearest-neighbor gold atoms. Reprinted with permission from Besenbacher *et al.* *Science* **279**, 1913 (1998). Copyright 1998 American Association for the Advancement of Science.

high reactivity with respect to the primary reaction channel, the methane decomposition. On the basis of DFT studies it was therefore suggested that the 2-D alloy of Au/Ni would be a better catalyst for methane dehydrogenation. Subsequent synthesis of an Au/Ni catalyst has shown this to be true (Fig. 37) (122).

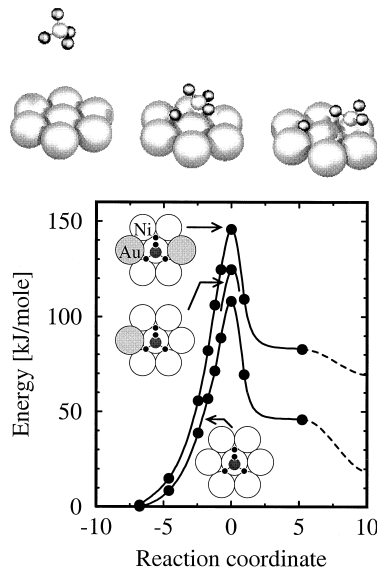


FIG. 36. Illustration of the calculated minimum energy path (reaction coordinate, in  $\text{\AA}$ ) for the  $\text{CH}_4$  dissociation on a  $\text{Ni}(111)$  surface. The energy (PW91) among the path is shown below. The shift in the barrier for dissociation when one or two gold atoms are nearest neighbors to the nickel atom under the dissociating  $\text{CH}_4$  molecule is also included. Adapted from Holmlund *et al.* (123).

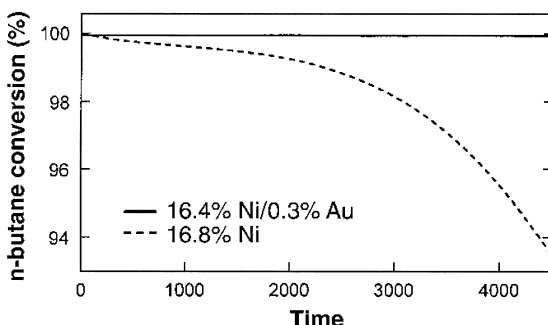


FIG. 37. Conversion of *n*-butane as a function of time (in seconds) during steam reforming in a 3% *n*-butane/7% hydrogen/3% water in helium mixture at a space velocity of  $1.2 \text{ h}^{-1}$ . The dashed curve shows the *n*-butane conversion for the nickel and the solid curve is for the gold/nickel supported catalyst. Reprinted with permission from Besenbacher *et al.* *Science* **279**, 1913 (1998). Copyright 1998 American Association for the Advancement of Science.

Several DFT calculations have been reported that show the effect of alloying on adsorption and reactions. Delbecq and Sautet (125, 126) investigated the bonding of CO and of NO on surfaces of Pd<sub>3</sub>Mn alloys. Pallassana *et al.* (127) also investigated the effect of alloying on hydrogen chemisorption on Pd–Re alloys and found that the adsorption energy varies with the average *d* band center, as has been previously determined.

The strong correlation between  $\epsilon_d$  and bond energies and activation barriers makes it interesting to have an overview of the way the *d* band centers change when one metal forms a monolayer on top of (or is alloyed into) the first layer of another metal. These shifts can be calculated by using the DFT, and Table II summarizes results for many combinations of catalytically interesting metals (128). We stress that the results are for

TABLE II  
*Shifts in d Band Centers of Surface Impurities and Overlays Relative to the Clean Metal Values (Bold)<sup>a</sup>*

	Fe	Co	Ni	Cu	Ru	Rh	Pd	Ag	Ir	Pt	Au
Fe	<b>-0.92</b>	0.05	-0.20	-0.13	-0.29	-0.54	-1.24	-0.83	-0.36	-1.09	-1.42
		0.14	-0.04	-0.05	-0.73	-0.72	-1.32	-1.25	-0.95	-1.48	-2.19
Co	0.01	<b>-1.17</b>	-0.28	-0.16	-0.24	-0.58	-1.37	-0.91	-0.36	-1.19	-1.56
		-0.01		-0.20	-0.06	-0.70	-0.95	-1.65	-1.36	-1.09	-2.39
Ni	0.09	0.19	<b>-1.29</b>	0.19	-0.14	-0.31	-0.97	-0.53	-0.14	-0.80	-1.13
		0.96	0.11		0.12	-0.63	-0.74	-1.32	-1.14	-0.86	-2.10
Cu	0.56	0.60	0.27	<b>-2.67</b>	0.58	0.32	-0.64	-0.70	0.58	-0.33	-1.09
		0.25	0.38	0.18		-0.22	-0.27	-1.04	-1.21	-0.32	-1.15
Ru	0.21	0.26	0.01	0.12	<b>-1.41</b>	-0.17	-0.82	-0.27	0.02	-0.62	-0.84
		0.30	0.37	0.29	0.30		-0.12	-0.47	-0.40	-0.13	-0.61
Rh	0.24	0.34	0.16	0.44	0.04	<b>-1.73</b>	-0.54	0.07	0.17	-0.35	-0.49
		0.31	0.41	0.34	0.22	0.03		-0.39	-0.08	0.03	-0.45
Pd	0.37	0.54	0.50	0.94	0.24	0.36	<b>-1.83</b>	0.59	0.53	0.19	0.17
		0.36	0.54	0.54	0.80	-0.11	0.25		0.15	0.31	-0.14
Ag	0.72	0.84	0.67	0.47	0.84	0.86	0.14	<b>-4.30</b>	1.14	0.50	-0.15
		0.55	0.74	0.68	0.62	0.50	0.67	0.27		0.80	0.37
Ir	0.21	0.27	0.05	0.21	0.09	-0.15	-0.73	-0.13	<b>-2.11</b>	-0.56	-0.74
		0.33	0.40	0.33	0.56	-0.01	-0.03	-0.42	-0.09		-0.49
Pt	0.33	0.48	0.40	0.72	0.14	0.23	-0.17	0.44	0.38	<b>-2.25</b>	-0.05
		0.35	0.53	0.54	0.78	0.12	0.24	0.02	0.19	0.29	
Au	0.63	0.77	0.63	0.55	0.70	0.75	0.17	0.21	0.98	0.46	<b>-3.56</b>
		0.53	0.74	0.71	0.70	0.47	0.67	0.35	0.12	0.79	0.43

<sup>a</sup> The impurity/overlayer atoms are listed horizontally, and the host entries are listed vertically. For each combination, the first of the two numbers listed represents the isolated surface impurity and the second the overlayer. The surfaces considered are the most close packed, and the overlayer structures are pseudomorphic. No relaxations from the host lattice positions are included. All values are in eV, and the elemental *d* band centers are relative to the Fermi level. From Ruban *et al.* (128).

overlayers and surface impurities occupying lattice positions of the substrate, and we have not taken into account here whether these structures are actually stable under experimental conditions. However, Table II can provide an idea about possible ways of modifying the electronic structure of a surface.

Consider for example the case of platinum on Au(111). According to the results of Table II, both platinum overlayers and platinum impurities in a Au(111) surface have higher-lying *d* states than platinum atoms in a Pt(111) surface and should therefore bind adsorbates more strongly and have lower transition state energies. We note that this may still lead to higher activation barriers for certain elementary steps if the initial state for this step is stabilized more than the transition state. The somewhat counterintuitive prediction that gold should *increase* the reactivity of platinum has been tested experimentally (102). In Fig. 38, it is clearly shown that CO is bonded more strongly to a monolayer of platinum on Au(111) than to Pt(111), in accordance with the prediction from Table II. The

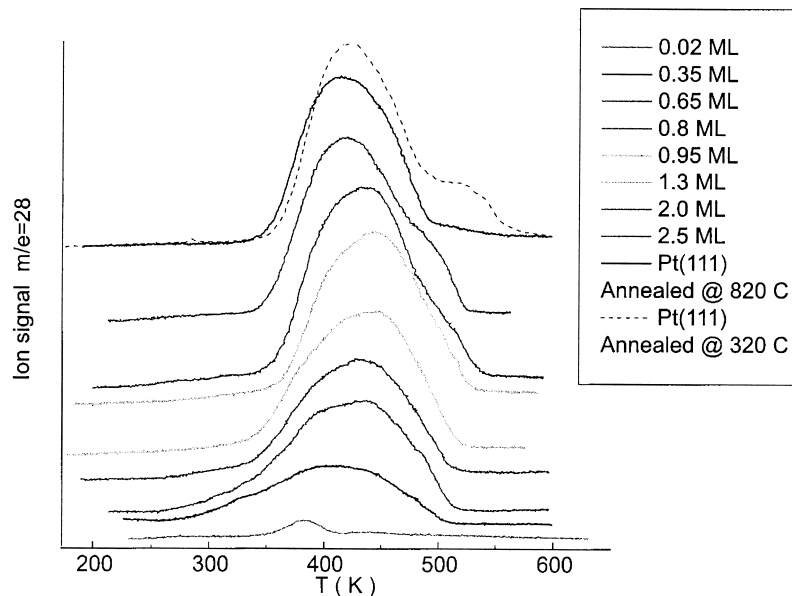


FIG. 38. CO thermal desorption spectra for different coverages of platinum Au(111). The spectrum for the clean Pt(111) surface is shown for comparison. Approximately one monolayer of platinum on the Au(111) surface is shown to bind CO more strongly (with a higher desorption temperature) than the clean Pt(111) surface. Reprinted from Pedersen *et al.* (102). Copyright 1999 with permission from Elsevier Science.

experimental results also show that platinum impurities do not bind CO as strongly as Pt(111). This would not be expected from Table II. This discrepancy can be traced to contributions to the bonding from second-nearest neighbors in the surface (102), and the example shows that one must be careful in using Table II when the second-nearest neighbors significantly change the reactivity. In the current case, platinum and gold are so different that even though only about 10% of the bonding comes from the second neighbors, it is enough to be important. This problem does not occur when pseudomorphic overlayers are considered.

It is known from several theoretical investigations that the variation in the center of the *d* bands for metal overlayers is accompanied by a similar variation in the surface core level shifts—at least toward the right in the transition metal series (129–131). It has also been shown that the *trends* in variations in the surface core level shifts for different overlayers are often given by the initial state shift, i.e., by the changes in the electronic structure of the unperturbed surface. Therefore, we conclude that we can view the variation in the surface core level shifts as a measure of the variation in the *d* band center. This is fortuitous because it means that in the surface core level shifts there is an *in situ* experimental measure of the valence *d* band center shifts that are important for the chemical properties of metal surfaces, as discussed previously. As an outstanding example of the information carried by the surface core level shifts, Rodriguez and Goodman (97), in their detailed studies of metallic overlayers, observed a strong correlation between the surface core level shift of such overlayers and the CO chemisorption energy at these overlayers.

When using Table II, for example, to decide which surface composition will be best for a given reaction, it must be borne in mind that the actual surface composition of a real catalyst particle cannot be varied at random. The tendency of one metal to segregate to the surface of another largely controls the surface composition. In the design of a catalyst, it therefore is of interest to have an overview of the tendency of different metals to segregate to the surface. Again, DFT calculations are a useful source of such information. Figure 39 shows a compilation of surface segregation energies of all transition metals (132). It can be seen from Fig. 39, for example, that even though the Pt/Au(111) system has interesting chemical properties is not a potential catalyst because the platinum is driven to the bulk by the energetics [the segregation energy for the Pt/Au(111) system is positive].

In many cases, alloying effects have been shown experimentally to change the reactivities of single-crystal surfaces (99, 133–135), and alloying effects have been explored extensively in catalyst development (136). Testing of such catalysts may benefit especially from new fast screening techniques

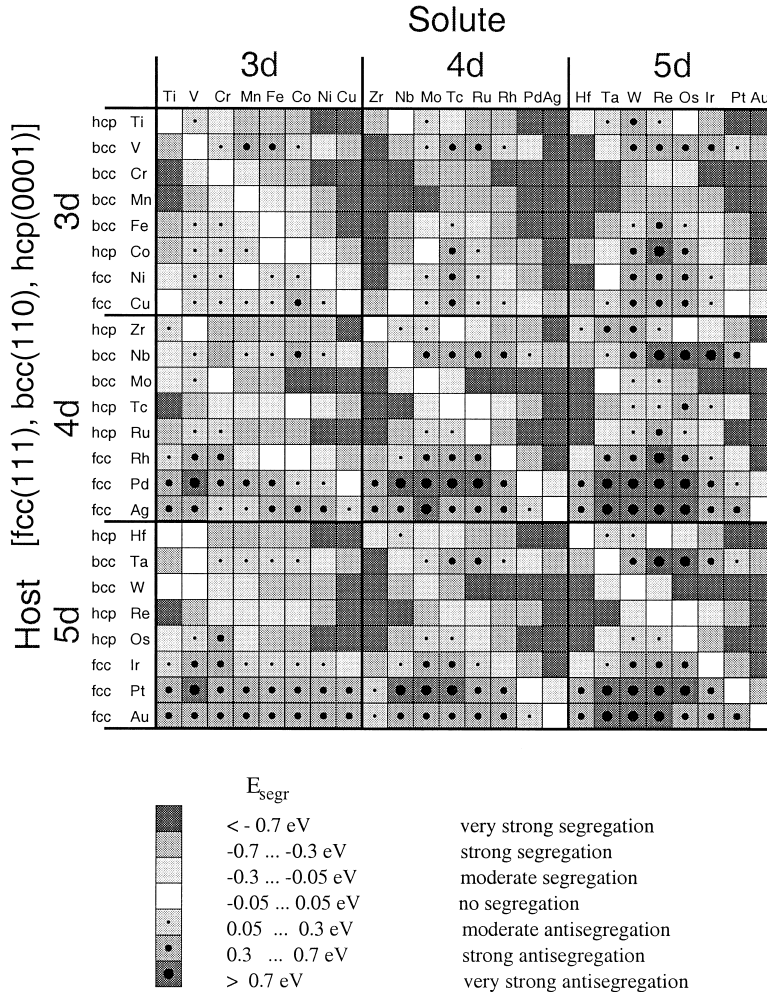


FIG. 39. Compilation of calculated segregation energies on the most close-packed surface of all binary combinations of transition metals. Adapted from Christensen *et al.* (132).

(137). The concepts developed previously, in conjunction with databases such as those in Fig. 39 and Table II, may be useful in guiding the choice of candidate combinations of metals to test experimentally.

### C. PROMOTION AND POISONING

The reactivity of a metal surface is modified by the presence of coadsorbates. Alkali metal adsorbates, for instance, are added to the iron- and

ruthenium-based industrial ammonia synthesis catalysts, causing an enhanced reactivity with respect to N<sub>2</sub> bond activation (138–140). Another example of a coadsorbate-modified catalyst is the nickel-based catalyst used in the SPARG process for steam reforming (124). In this process, H<sub>2</sub>S is added to the feed gas flow, resulting in adsorbed sulfur atoms that inhibit coking of the surface in much the same way that gold inhibits coking in the Au/Ni catalyst discussed previously.

The interaction of identical coadsorbates was considered in Section III.C, and four different interaction types were described. The direct overlap of orbitals is operative for small adsorbate–adsorbate distances. It always occurs and is usually repulsive. The same is true of the indirect elastic interaction through the substrate. The other two interaction types are more interesting:

- Indirect interaction through the metal *d* bands
- Direct electrostatic interaction

The indirect interaction through the metal *d* bands is illustrated in Fig. 40 (141). Here, the Ru 4*d* bands at a ruthenium atom next to a threefold site are shown before and after the adsorption of sulfur in the threefold site. Figure 40 shows how the ruthenium 4*d* band center is shifted down upon adsorption of sulfur. The sulfur atom effectively provides some of the coordination that a ruthenium atom in the surface lacks. Once the ruthenium atom is more highly coordinated, the *d* band width of the surface atom increases and the *d* band shifts down. This electronic effect weakens the bonding of other adsorbates in sites involving ruthenium atoms that have

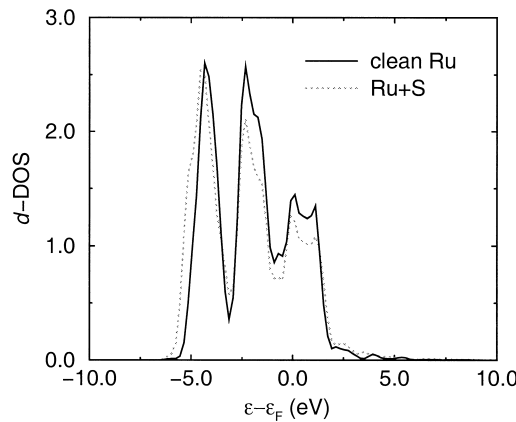


FIG. 40. The Ru(0001) *d* DOS including the effect of sulfur. Adapted from Mortensen *et al.* (141).

already reacted. For  $\text{N}_2$  dissociation on a Ru(0001) surface with coadsorbed sulfur, the energy barrier is increased substantially by the presence of the surface sulfur atoms (Fig. 41). Farther away, the effect is weaker, however, because it involves only the shift of  $d$  bands at immediate surface neighbor atoms.

So far, we have implicitly assumed that the changes in adsorbate bond strengths and energy barriers resulting from changes in the electronic structure of a metal surface can be traced to the Kohn–Sham eigenvalue spectra of the DFT calculations, i.e., to the change in the sum of Kohn–Sham eigen energies resulting from adsorption,  $\Delta \sum_i \varepsilon_i$ . A formal derivation, however, reveals that electronic structure changes may also be manifest in changes of the (nonlocal) electrostatic contributions,  $\Delta E_{es}$ , to the adsorbate bond strengths and energy barriers (40, 44, 142). The potential energy change from the electronic effect must therefore be written as follows:

$$\Delta E_a = \Delta \sum_i \varepsilon_i + \Delta E_{es}. \quad (2)$$

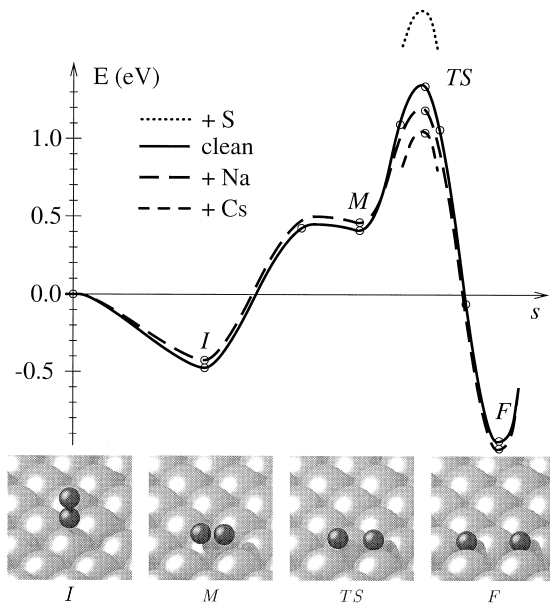


FIG. 41. (Bottom) Snapshots of the minimum energy path for the  $\text{N}_2$  dissociation reaction: Initial state in which the molecule is standing perpendicular to the surface ( $I$ ), metastable state ( $M$ ), transition state ( $TS$ ), and final state ( $F$ ). (Top) The energy along the path. The effect on the transition state of adding one-eighth of a monolayer of sulfur or sodium or one-sixth of a monolayer of cesium is also shown. Adapted from Mortensen *et al.* (141).

When sodium or cesium is adsorbed on Ru(0001), there is no *d* band shift (relative to the Fermi level) at ruthenium sites farther than one lattice constant away. Consequently, the first term in Eq. (2) is approximately zero. Because of charge transfer from the alkali metal adsorbates to the ruthenium surface, however, there are electrostatic effects. This is shown in Fig. 42, in which the *d* bands are shown to be essentially unchanged, whereas an electrostatic field,  $E$ , has been induced outside the ruthenium surface. In Fig. 41 the result of a full DFT description of the  $N_2$  dissociation on a Ru(0001) surface with coadsorbed sodium or cesium is also shown. The energy barrier is reduced by some amount  $|\Delta E_{TS}|$  as a consequence of the presence of either sodium or cesium. These atoms thus act as promoters for the  $N_2$  bond activation. The effect can be traced to the electrostatic interaction between the dipole,  $\mu$ , of the  $N_2$  transition state complex interacting with the induced electrostatic field,  $E$ , due the adsorbed alkali atoms.

In Fig. 43,  $\Delta E_{TS}$  is plotted as a function of the quantity

$$\Delta E_{\text{dip}} = -E\mu. \quad (3)$$

A clear correlation is evident, confirming that the electrostatic interaction is dominating (143).

In the examples discussed previously, special care was taken to consider low coverages of poisons or promoters. This is usually the situation encoun-

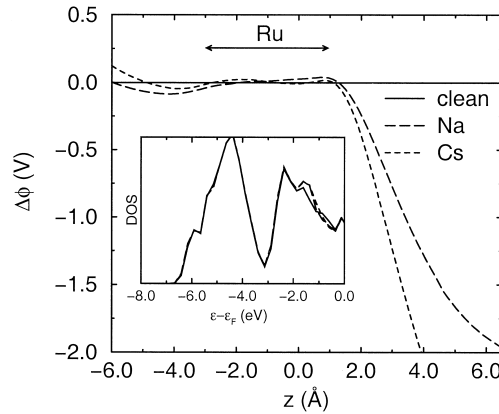


FIG. 42. Calculated change in the electrostatic potential outside a Ru(0001) surface as a result of the adsorption of a sodium or a cesium atom. The potential is shown along a line perpendicular to the ruthenium surface at a site 5.48 Å from the alkali metal atom. In the inset, the *d* DOS is shown with (dashed line) and without (solid line) the sodium illustrating that the *d* DOS is almost unaffected by the presence of the alkali metal atom. From Mortensen *et al.* (141).

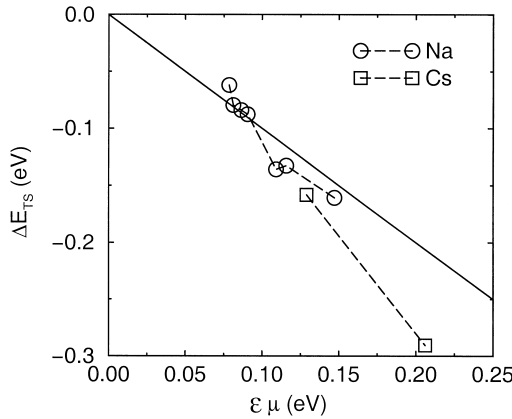


FIG. 43. Interaction energy between alkali metal atoms and  $N_2$  in the transition state for dissociation as a function of  $\varepsilon \mu$ . The alkali metal atoms are sodium (circles) and cesium (squares). Many different geometries have been considered corresponding to different distances between the transition state complex and the alkali metal atoms. Adapted from Mortensen *et al.* (141).

tered in practical catalysis, and it singles out the long- and short-range effects as well. If one instead considers high coverages, one finds that all the interaction types work simultaneously, and the picture becomes much more complicated (144, 145).

## VI. Summary and Extension of Concepts to Metal Sulfides

Density functional calculations of adsorption and reactions at metal surfaces have reached a point at which the complexity of real catalytic surfaces and adsorbates can be treated at a level of accuracy that is sufficient for understanding bonding mechanisms, for determining reaction pathways, and for comparing different systems. The calculations therefore provide a new and powerful source of input to the description of heterogeneous catalysis. The calculations will never replace experiments, but they may in many cases be the simplest or even the only possible way of obtaining some information.

The calculations also provide new ways of testing whether the concepts we use to describe surface chemical processes are correct. For instance, it has been shown in this way that earlier reactivity measures such as the density of states at the Fermi level or the number of  $d$  holes cannot in general describe variations in reactivity from one transition metal to the next (45).

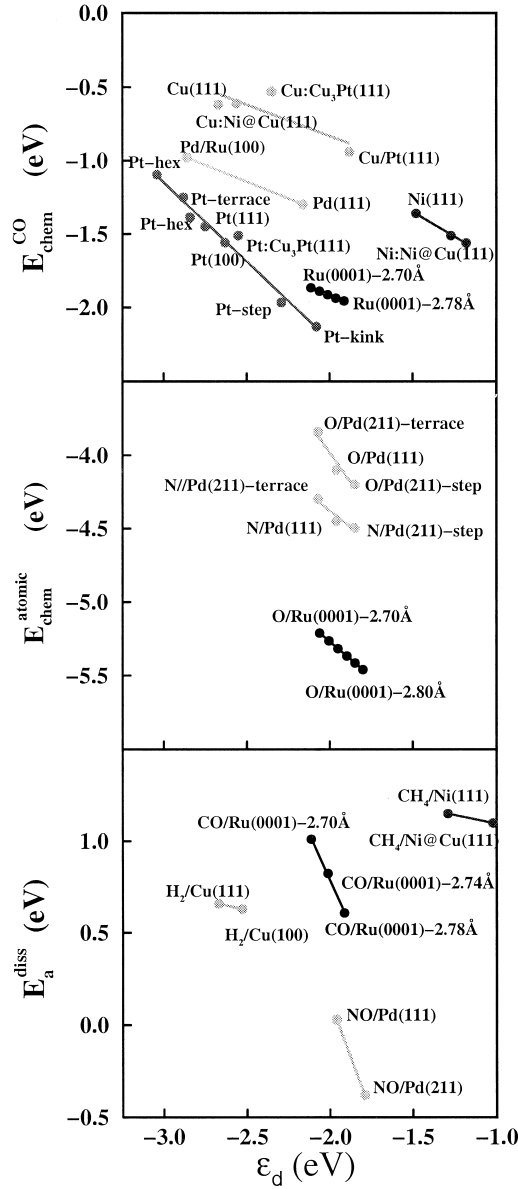


FIG. 44. Molecular ( $E_{\text{chem}}^{\text{CO}}$ ) and atomic ( $E_{\text{chem}}^{\text{atomic}}$ ) binding energy as a function of the  $d$  band center ( $\varepsilon_d$ ) of the metal surface (top and middle, respectively). The barrier for dissociation of small molecules, referred to gas-phase zero, as a function of  $\varepsilon_d$  is shown in the bottom. Common shadings are used for data corresponding to the same metal in each of the three panels. Lines drawn represent best linear fits.  $X:XY$  reflects chemisorption or dissociation at atom  $X$  in an  $XY$ -alloy surface.  $X@Y$  means an  $X$  atom impurity in a  $Y$  surface. From Mavrikakis *et al.* (14).

In this review, we have focused on some simple concepts that can be used to classify the reactivities of transition metal surfaces. The goal is to gain an understanding of the properties of the clean surface that determine its reactivity. If we can single out these factors, we have powerful concepts that can be used to develop new and more effective catalysts.

We have shown that electronic and geometrical factors can be separated and that both are important in determining the reactivity. The main conclusion of our work is that when considering variations in the reactivity of a particular metal or group of metals, a single parameter, the center of the  $d$  band ( $\varepsilon_d$ ), is strongly related to both the stabilities of atoms and molecules on the surface and the energies of transition states for surface processes. A summary of many calculations illustrating this point is shown in Fig. 44. We have shown in detail why this is the case, and we have shown what determines variations in  $\varepsilon_d$ ; low-coordinated or “expanded” metal atoms are more reactive than highly coordinated or “compressed” metal atoms.

These concepts have been developed specifically for transition metal surfaces, but there are good reasons to believe that they are more general. To exemplify this, we show here as the final example how very similar concepts can be used to understand the reactivities of transition metal sulfides.  $\text{MoS}_2$  (on supports) is used, extensively as a catalyst for hydrotreating processes. It is known that cobalt and nickel promote the catalysts, whereas iron (next to these elements in the periodic table) does not. It is also known that the promoter atoms are situated at the perimeter of the supported  $\text{MoS}_2$  nanoparticles. In this connection, it is interesting to know

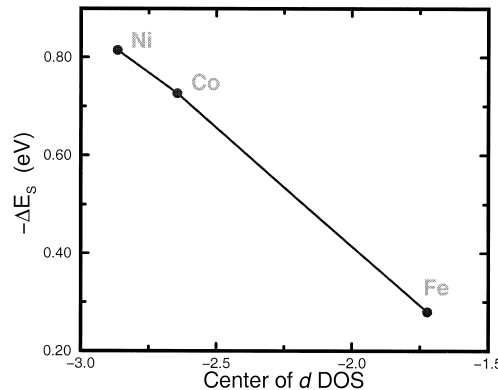


FIG. 45. Plot of the change in the S-binding energy to the edge of a  $\text{MoS}_2$  slab, with Fe, Co, and Ni substituted for one of the Mo atoms next to the S atom in question. The result is shown as a function of the center of the projected  $d$  density of states on the Fe, Co, or Ni atoms in questions. From Byskov *et al.* (146).

how iron, cobalt, and nickel affect the stability of edge sulfur atoms. If, for example, the sulfur atoms are more easily removed in the presence of cobalt, this might create more active sites with coordinatively unsaturated metal atoms and thus explain the promoting effect. In Fig. 45, the variations in the calculated sulfur binding energy (the reaction energy for H<sub>2</sub>S formation from H<sub>2</sub>) for different promoter atoms are shown. Again, the variations correlate with the position of the *d* band center.

#### ACKNOWLEDGMENTS

We thank many colleagues and collaborators for contributing to the work described in this review, including H. Bengaard, F. Besenbacher, L. Byskov, I. Chorkendorff, B. S. Clausen, J. A. Dumesic, M. V. Ganduglia-Pirovano, A. Groß, L. B. Hansen, K. W. Jacobsen, P. Kratzer, J. H. Larsen, A. Logadottir, B. I. Lundqvist, E. Lægsgaard, M. Mavrikakis, Y. Morikawa, J. J. Mortensen, M. Neurock, O. H. Nielsen, V. Pallassana, J. Rostrup-Nielsen, A. Ruban, M. Scheffler, H. L. Skriver, Ž. Šljivančanin, I. Stensgaard, K. Stokbro, P. Stoltze, E. Törnqvist, H. Topsøe, R. M. Watwe, and J. T. Yates. JKN gratefully acknowledges the hospitality of H. Metiu and the support from the Center for Quantized Electronic Structures, University of California, Santa Barbara, during the writing of the manuscript. This work was in part financed by the Danish Research Councils through The Center for Surface Reactivity and Grants 9501775, 9800425, and 9803041. The Center for Atomic-Scale Materials Physics is sponsored by the Danish National Research Foundation.

#### REFERENCES

1. Barateau, A. M., and Vohs, J. M., in "Handbook of Heterogeneous Catalysis" (G. Ertl, H. Knözinger, and J. Weitkamp, Eds.), p. 873. VCH, Weinheim, 1997.
2. Somorjai, G. A., in "Introduction of Surface Chemistry and Catalysis." Wiley, New York, 1994.
3. Gunter, P. L. J., Niemantsverdriet, J. W., Ribeiro, F., and Somorjai, G. A., *Catal. Rev.—Sci. Eng.* **39**, 77 (1997).
4. Cambell, C. T., *Surf. Sci. Rep.* **27**, 1 (1997).
5. Valden, M., Lai, X., and Goodman, D. W., *Science* **281**, 1647 (1998).
6. Henry, C. R., *Surf. Sci. Rep.* **31**, 235 (1998).
7. Sandell, A., Libuda, J., Brühwiler, P. A., Andersson, S., Maxwell, A. J., Bäumer, M., Mårtensson, N., Freund, H.-J., *J. Vac. Sci. Technol. A* **14**, 1546 (1996).
8. Højrup Hansen, K., Worren, T., Stempel, S., Lægsgaard, E., Bäumer, M., Freund, H.-J., Besenbacher, F., and Stensgaard, I., *Phys. Rev. Lett.* **83**, 4120 (1999).
9. Clausen, B. S., Topsøe, H., and Frahm, R., *Adv. Catal.* **42**, 315 (1998).
10. Thomas, J. M., and Lambert, R. M. (Eds.), "Characterization of Catalysts." Wiley, New York, 1980.
11. Delgass, W. N., Haller, G. L., Kellerman, R., and Lunsford, J. H. (Eds.), "Spectroscopy in Heterogeneous Catalysis." Academic Press, New York, 1979.
12. Niemantsverdriet, J. W., "Spectroscopy in Catalysis: An Introduction." VCH, Weinheim, 1993.
13. Vitos, L., Ruban, A. V., Skriver, H., and Kollar, J., *Surf. Sci.* **411**, 186 (1998).
14. Mavrikakis, M., Hammer, B., and Nørskov, J. K., *Phys. Rev. Lett.* **81**, 2819 (1998).
15. Here, W. J., Radom, L., Schleyer, P. v. R., and Pople, J. A., "Ab Initio Molecular Orbital Theory." Wiley, New York, 1987.

16. Hohenberg, P., and Kohn, W., *Phys. Rev.* **136**, B864 (1964); Kohn, W., and Sham, L., *Phys. Rev.* **140**, A1133 (1965).
17. Payne, M. C., Teter, M. P., Allan, D. C., Arias, T. A., and Joannopoulos, J. D., *Rev. Mod. Phys.* **64**, 1045 (1992).
18. Kresse, G., and Furthmüller, J., *Comput. Mat. Sci.* **6**, 15 (1996).
19. Yang, H., and Whitten, J. L., *J. Chem. Phys.* **96**, 5529 (1992).
20. Inglesfield, J. E., and Benesh, G. A., *Phys. Rev. B* **37**, 6682 (1988).
21. MacLaren, J. M., Crampin, S., Vvedensky, D. D., and Pendry, J. B., *Phys. Rev. B* **40**, 12164 (1989).
22. Skriver, H. L., and Rosengaard, N. M., *Phys. Rev. B* **43**, 9538 (1991).
23. Vanderbilt, D., *Phys. Rev. B* **41**, 7892 (1990).
24. Blöchl, P. E., *Phys. Rev. B* **50**, 17953 (1994).
25. Becke, A. D., *J. Chem. Phys.* **98**, 5648 (1993).
26. Perdew, J. P., Chevary, J. A., Vosko, S. H., Jackson, K. A., Pederson, M. R., Singh, D. J., and Fiolhais, C., *Phys. Rev. B* **46**, 6671 (1992).
27. Perdew, J. P., Burke, K., and Ernzerhof, M., *Phys. Rev. Lett.* **77**, 3865 (1996).
28. Hammer, B., Hansen, L. B., and Nørskov, J. K., *Phys. Rev. B* **59**, 7413 (1999).
29. Hammer, B., Jacobsen, K. W., and Nørskov, J. K., *Phys. Rev. Lett.* **70**, 3971 (1993).
30. Philipsen, P. H. T., te Velde, G., and Baerends, E. J., *Chem. Phys. Lett.* **226**, 583 (1994).
31. Hu, P., King, D. A., Crampin, S., Lee, M.-H., and Payne, M. C., *Chem. Phys. Lett.* **230**, 501 (1994).
32. Hammer, B., Scheffler, M., Jacobsen, K. W., and Nørskov, J. K., *Phys. Rev. Lett.* **73**, 1400 (1994).
33. White, J. A., Bird, D. M., Payne, M. C., and Stich, I., *Phys. Rev. Lett.* **73**, 1404 (1994).
34. Brown, W. A., Kose, R., and King, D. A., *Chem. Rev.* **98**, 797 (1998).
35. Pettifor, D., "Bonding and Structure of Molecules and Solids," Clarendon, Oxford, 1995.
36. Lundqvist, B. I., Gunnarsson, O., Hjelmberg, H., and Nørskov, J. K., *Surf. Sci.* **89**, 196 (1979).
37. Newns, D. M., *Phys. Rev.* **178**, 1123 (1969); Grimley, T. B., *J. Vac. Sci. Techno.* **8**, 31 (1971); **9**, 561 (1971).
38. Hammer, B., *Faraday Discuss.* **110**, 323 (1998).
39. Starke, U., Van Hove, M. A., and Somorjai, G. A., *Prog. Surf. Sci.* **46**, 305 (1994).
40. Hammer, B., and Nørskov, J. K., in "Chemisorption and Reactivity on Supported Clusters and Thin Films" (R. M. Lambert and G. Pacchioni, Eds.), pp. 285–351. Kluwer Academic, Dordrecht, 1997.
41. Bogicevic, A., Stromquist, J., and Lundqvist, B. I., *Phys. Rev. B* **57**, R4289 (1998).
42. Steininger, H., Lehwald, S., and Ibach, H., *Surf. Sci.* **123**, 1 (1982).
43. Nørskov, J. K., *Rep. Prog. Phys.* **53**, 1253 (1990).
44. Holloway, S., Lundqvist, B. I., and Nørskov, J. K., in "Proceedings of the International Congress on Catalysis," Vol. 4, p. 85, Verlag Chemie Weinheim Berlin, 1984.
45. Hammer, B., and Nørskov, J. K., *Surf. Sci.* **343**, 211 (1995); **359**, 306 (1996).
46. Hammer, B., and Nørskov, J. K., *Nature* **376**, 238 (1995).
47. Mortensen, J. J., Morikawa, Y., Hammer, B., and Nørskov, J. K., *J. Catal.* **169**, 85 (1997).
48. Stokbro, K., and Baroni, S., *Surf. Sci.* **370**, 166 (1997).
49. Toyoshima, I., and Somorjai, G. A., *Catal. Rev. Eng.* **19**, 105 (1979).
50. Andersen, O. K., Jepsen, O., and Glotzel, D., in "Highlights of Condensed Matter Theory," LXXXIX, p. 59. Corso Soc. Italiana di Fisica, Bologna, 1985.
51. Hoffmann, R., *Rev. Mod. Phys.* **60**, 601 (1988).
52. Bagus, P. S., and Pacchioni, G., *Surf. Sci.* **278**, 427 (1992).
53. Blyholder, G., *J. Phys. Chem.* **68**, 2772 (1964).

54. Van Santen, R. A., and Neurock, M., *Catal. Rev.—Sci. Eng.* **37**, 557 (1995).
55. Hammer, B., Morikawa, Y., and Nørskov, J. K., *Phys. Rev. Lett.* **76**, 2141 (1996).
56. Loffreda, D., Simon, D., and Sautet, P., *J. Chem. Phys.* **108**, 6447 (1998).
57. Broden, G., Rhodin, T. N., Brukner, C., Benbow R., and Hurysh, Z., *Surf. Sci.* **59**, 593 (1976).
58. Pallassana, V., and Neurock, M., *J. Catal.* in press (2000).
59. Ge, Q., and King, D. A., *J. Chem. Phys.* **110**, 4699 (1999).
60. Mortensen, J. J., Ganduglia-Pirovano, M. V., Hansen, L. B., Hammer, B., Stoltze, P., and Nørskov, J. K., *Surf. Sci.* **422**, 8 (1999).
61. Bozso, F., Ertl, G., Grunze, M., and Weiss, M., *J. Catal.* **49**, 18 (1977); Imbihl, R., Behm, R. J., Ertl, G., and Moritz, W., *Surf. Sci.* **123**, 129 (1982).
62. Stampfl, C., Schwegmann, S., Over, H., Scheffler, M., and Ertl, G., *Phys. Rev. Lett.* **77**, 3371 (1996).
63. Stampfl, C., Kreuzer, H. J., Payne, S. H., Pfünfer, H., and Scheffler, M., *Phys. Rev. Lett.* **83**, 2993 (1999).
64. Diekhöner, L., Baurichter, A., Mortensen, H., and Luntz, A. C., submitted for publication.
65. Ge, Q., King, D. A., Lee, M.-H., White, J. A., and Payne, M. C., *J. Chem. Phys.* **106**, 1210 (1997).
66. Hammer, B., and Nørskov, J. K., *Phys. Rev. Lett.* **79**, 4441 (1997).
67. Lau, K. H., and Kohn, W., *Surf. Sci.* **65**, 607 (1977).
68. Österlund, L., Pedersen, M. Ö., Stensgaard, I., Lægsgaard, E., and Besenbacher, F., *Phys. Rev. Lett.* **83**, 4812 (1999).
69. Bradley, J. M., Hopkinson, A., and King, D. A., *J. Phys. Chem.* **99**, 17032 (1995).
70. Somorjai, G. A., and Borodko, Y., *Catal. Lett.* **59**, 89 (1999).
71. Murphy, M. J., Skelly, J. F., Hodgson, A., and Hammer, B., *J. Chem. Phys.* **110**, 6954 (1999).
72. Darling, G. R., and Holloway, S., *Rep. Prog. Phys.* **58**, 1595 (1995).
73. Groß, A., *Surf. Sci. Rep.* **32**, 291 (1998).
74. Kroes, G. J., *Prog. Surf. Sci.* **60**, 1 (1999).
75. Mavrikakis, M., Hansen, L. B., Mortensen, J. J., Hammer, B., and Nørskov, J. K., in “Transition State Modelling for Catalysis” (D. G. Truhlar and K. Morokuma, Eds.), ACS Symposium Series, 721, Oxford University Press, 1999.
76. van Daelen, M. A., Li, Y. S., Newsam, J. M., and van Santen, R. A., *Chem. Phys. Lett.* **266**, 100 (1994).
77. Eichler, A., and Hafner, J., *Phys. Rev. Lett.* **79**, 4481 (1997).
78. Gravil, P. A., Bird, D. M., and White, J. A., *Phys. Rev. Lett.* **77**, 3933 (1996).
79. Alavi, A., Hu, P., Deutsch, T., Silvestrelli, P. L., and Hutter, J., *Phys. Rev. Lett.* **80**, 3650 (1998).
80. Eichler, A., and Hafner, J., *Phys. Rev. B* **59**, 5960 (1999).
81. Stampfl, C., and Scheffler, M., *Phys. Rev. Lett.* **78**, 1500 (1997).
82. Watwe, R. M., Cortright, R. D., Nørskov, J. K., and Dumesic, J. A., to be published.
83. Dahl, S., Logadottir, A., Egeberg, R. C., Larsen, J. H., Chrokendorff, I., Törnqvist, E., and Nørskov, J. K., *Phys. Rev. Lett.* **83**, 1814 (1999).
84. Hammer, B., *Phys. Rev. Lett.* **83**, 3681 (1999).
85. Morikawa, Y., Mortensen, J. J., Hammer, B., and Nørskov, J. K., *Surf. Sci.* **386**, 67 (1997).
86. Kratzer, P., Hammer, B., and Nørskov, J. K., *J. Chem. Phys.* **105**, 5595 (1996).
87. Berger, H. F., Leisch, M., Winkler, A., and Rendulic, K., *Chem. Phys. Lett.* **175**, 425 (1985); Robota, H. J., Vielhaber, W., Lin, M. C., Segner, J., and Ertl, G., *Surf. Sci.* **155**, 101 (1985).
88. Brown, J. K., Luntz, A., and Schultz, P. A., *J. Chem. Phys.* **95**, 3767 (1991).

89. Hayden, B. E., and Lamont, C. L., *Phys. Rev. Lett.* **63**, 1823 (1989); Rasmussen, P. B., Holmblad, P. M., Christoffersen, H., Taylor, P. A., and Chorkendorff, I., *Surf. Sci.* **287/288**, 79 (1993).
90. Sault, A. G., Madix, R. J., and Cambell, C. T., *Surf. Sci.* **169**, 347 (1986).
91. Eichler, A., Kresse, G., and Hafner, J., *Surf. Sci.* **397**, 116 (1998).
92. Wilke, S., and Scheffler, M., *Phys. Rev. B* **53**, 4926 (1996).
93. Groß, A., Wilke, S., and Scheffler, M., *Phys. Rev. Lett.* **75**, 2718 (1995).
94. White, J. A., Bird, D. M., and Payne, M. C., *Phys. Rev. B* **53**, 1667 (1996).
95. Kay, M., Darling, G. R., Holloway, S., White, J. A., and Bird, D. M., *Chem. Phys. Lett.* **245**, 311 (1995).
96. Gsell, M., Jakob, P., and Menzel, D., *Science* **280**, 717 (1998).
97. Rodriguez, J. A., and Goodman, D. W., *Science* **257**, 897 (1992).
98. Madey, T. E., Nien, C.-H., Pelhos, K., Kolodziej, J. J., Abdelrehim, I. M., and Tao, H.-S., *Surf. Sci.* **438**, 191 (1999).
99. Bautier de Mongeot, F., Scherer, M., Gleich, B., Kopatzki, E., and Behm, R. J., *Surf. Sci.* **411**, 249 (1998).
100. Kampshoff, E., Hahn, E., and Kern, K., *Phys. Rev. Lett.* **73**, 704 (1994).
101. Larsen, J. H., and Chorkendorff, I., *Surf. Sci.* **405**, 62 (1998).
102. Pedersen, M. Ø., Helveg, S., Ruban, A., Stensgaard, I., Lægsgaard, E., Nørskov, J. K., and Besenbacher, F., *Surf. Sci.* **426**, 395 (1999).
103. Zambelli, T., Wintterlin, J., and Ertl, G., to be published.
104. Logadottir, A., to be published.
105. Clausen, B. S., and Nørskov, J. K., *Topics Catal.*, in press (1999).
106. Klimenkov, M., Nepijko, S., Kuhlenbeck, H., Baumer, M., Schlögl, R., and Freund, H.-J., *Surf. Sci.* **391**, 27 (1997); Nepijko, S., Klimenkov, M., Kuhlenbeck, H., Zemlyanov, D., Herein, D., Schlögl, R., and Freund, H.-J., *Surf. Sci.* **412/413**, 192 (1998).
107. Giorgio, S., Chapon, C., Henry, C. R., Nihoul, G., and Penisson, J. M., *Phil. Mag. A* **64**, 87 (1991).
108. Hammer, B., Nielsen, O. H., and Nørskov, J. K., *Catal. Lett.* **46**, 31 (1997).
109. Kratzer, P., Hammer, B., and Nørskov, J. K., *Surf. Sci.* **359**, 45 (1996).
110. Hammer, B., *Surf. Sci.*, in press (2000).
111. Feibelman, P. J., Esch, S., and Michely, T., *Phys. Rev. Lett.* **77**, 2257 (1996).
112. Tripa, C. E., Zubkov, T. S., Yates, J. T., Mavrikakis, M., and Nørskov, J. K., *J. Chem. Phys.* **111**, 8651 (1999).
113. Bengaard, H. S., Rostrup-Nielsen, J. R., and Nørskov, J. K., to be published.
114. Ramsier, R. D., Gao, Q., Neergaard Waltenburg, H., and Yates, J. T., Jr., *J. Chem. Phys.* **100**, 6837 (1994).
115. Kose, R., Brown, W. A., and King, D. A., *J. Am. Chem. Soc.* **121**, 4845 (1999).
116. Zambelli, T., Wintterlin, J., Trost, J., and Ertl, G., *Science* **273**, 1688 (1996).
117. Dietrich, H., Geng, P., Jacobi, K., and Ertl, G., *J. Chem. Phys.* **104**, 375 (1996).
118. Taylor, H. S., *Proc. R. Soc. London A* **108**, 105 (1925).
119. Boudart, M., *Adv. Catal. Relat. Subj.* **20**, 153 (1969).
120. Shekhar, R., and Bartea, M. A., *Catal. Lett.* **31**, 221 (1995).
121. Hammer, B., and Scheffler, M., *Phys. Rev. Lett.* **74**, 3487 (1995).
122. Besenbacher, F., Chorkendorff, I., Clausen, B. S., Hammer, B., Molenbroek, A., Nørskov, J. K., and Stensgaard, I., *Science* **279**, 1913 (1998).
123. Holmblad, P. M., Hvolbæk Larsen, J., Chorkendorff, I., Nielsen, L. P., Besenbacher, F., Stensgaard, I., Lægsgaard, E., Kratzer, P., Hammer, B., and Nørskov, J. K., *Catal. Lett.* **40**, 131 (1996).

124. Rostrup-Nielsen, J., *J. Catal.* **85**, 31 (1994); Andersen, N. T., Topsøe, F., Alstrup, I., and Rostrup-Nielsen, J., *J. Catal.* **104**, 454 (1987).
125. Delbecq, F., and Sautet, P., *Chem. Phys. Lett.* **302**, 91 (1999).
126. Delbecq, F., and Sautet, P., *Phys. Rev. B* **59**, 5142 (1999).
127. Pallassana, V., Neurock, M., Hansen, L. B., Hammer, B., and Nørskov, J. K., *Phys. Rev. B* **60**, 6146 (1999); Pallassana, V., Neurock, M., Hansen, L. B., and Nørskov, J. K., to be published.
128. Ruban, A., Hammer, B., Stoltze, P., Skriver, H. L., and Nørskov, J. K., *J. Mol. Catal. A* **115**, 421 (1997).
129. Weinert, M., and Watson, R. E. *Phys. Rev. B* **51**, 17168 (1995).
130. Hennig, D., Ganduglia-Pirovano, M. V., and Scheffler, M., *Phys. Rev. B* **53**, 10344 (1996).
131. Ganduglia-Pirovano, M. V., Natoli, V., Cohen, M. H., Kudrnovsky, J., and Turek, I., *Phys. Rev. B* **54**, 8892 (1996).
132. Christensen, A., Ruban, A. V., Stoltze, P., Jacobsen, K. W., Skriver, H. L., Nørskov, J. K., and Besenbacher, F., *Phys. Rev. B* **56**, 5822 (1997); Ruban, A. V., Skriver, H. L., and Nørskov, J. K., *Phys. Rev. B*, **59**, 15900 (1999).
133. Bertolini, J. C., Tardy, B., Abon, M., Billy, J., Delichere, P., and Massardier J. *Surf. Sci.* **135**, 117 (1983).
134. Nieuwenhuys, B. E., *Surf. Rev. Lett.* **3**, 1869 (1996).
135. Linke, R., Schneider, U., Busse, H., Becker, C., Schröder, U., Castro, G. R., and Wandelt, K., *Surf. Sci.* **307–309**, 4074 (1994).
136. Sinfelt, J. H., "Bimetallic Catalysts: Discoveries, Concepts, and Applications." Wiley, New York, 1983; Ponec, V., *Adv. Catal.* **32**, 149 (1983).
137. Cong, P., Doolen, R. D., Fan, Q., Giaquinta, D. M., Guan, S., McFarland, E. W., Poojary, D. M., Selt, K., Turner, H. W., and Weinberg, W. H., *Angew. Chem., Int. Ed. Engl.*, **38**, 484 (1999).
138. Jennings, J. R. (Ed.), "Catalytic Ammonia Synthesis." Plenum, New York, 1991; H. Topsøe, H. Boudart, and J. K. Nørskov (Eds.), *Topics Catal.* **1**, 185–415 (1994).
139. Ertl, G., Lee, S. B., and Weiss, M., *Surf. Sci.* **111**, L711 (1981); Ertl, G., *Catal. Rev.—Sci. Eng.* **21**, 201 (1980).
140. Spencer, N. D., Schoonmaker, R. C., and Somorjai, G. A., *J. Catal.* **74**, 129 (1982).
141. Mortensen, J. J., Hammer, B., and Nørskov, J. K., *Phys. Rev. Lett.* **80**, 4333 (1998); Mortensen, J. J., Hammer, B., and Nørskov, J. K., *Surf. Sci.* **414**, 315 (1998).
142. Jacobsen, K. W., Nørskov, J. K., and Puska, M. J., *Phys. Rev. B* **35**, 7423 (1987).
143. Nørskov, J. K., Holloway, S., and Lang, N. D., *Surf. Sci.* **137**, 65 (1984); Nørskov, J. K., in "Physics and Chemistry of Alkali Metal Adsorption" (H. P. Bonzel, A. M. Bradshaw, and G. Ertl, Eds.), p. 253. Elsevier, Amsterdam, 1989.
144. Wilke, S., and Scheffler, M., *Phys. Rev. Lett.* **76**, 3380 (1996).
145. Wilke, S., and Cohen, M. H., *Surf. Sci.* **380**, 1441 (1997).
146. Byskov, L., Clausen, B. S., Topsøe, H., and Nørskov, J. K., *J. Catal.* **187**, 109 (1999).